Neurobiology of Disease

TSG-6–Mediated Extracellular Matrix Modifications Regulate Hypoxic–Ischemic Brain Injury

Taasin Srivastava,[1] Hung Nguyen,[2] Gage Haden,[1] Parham Diba,[1] Steven Sowa,[1] Norah LaNguyen,[1] William Reed-Dustin,[1] Wenbin Zhu,[2] Xi Gong,[1] Edward N. Harris,[3] Selva Baltan,[2] and Stephen A. Back[1,4]

[1]Department of Pediatrics, Oregon Health and Science University (OHSU), Portland, Oregon 97239, [2]Division of Anesthesiology and Perioperative Medicine (APOM), Oregon Health and Science University (OHSU), Portland, Oregon 97239, [3]Department of Biochemistry, University of Nebraska-Lincoln, Lincoln, Nebraska 68588, and [4]Department of Neurology, Oregon Health and Science University (OHSU), Portland, Oregon 97239

Proteoglycans containing link domains modify the extracellular matrix (ECM) to regulate cellular homeostasis and can also sensitize tissues/organs to injury and stress. Hypoxic–ischemic (H–I) injury disrupts cellular homeostasis by activating inflammation and attenuating regeneration and repair pathways. In the brain, the main component of the ECM is the glycosaminoglycan hyaluronic acid (HA), but whether HA modifications of the ECM regulate cellular homeostasis and response to H–I injury is not known. In this report, employing both male and female mice, we demonstrate that link-domain–containing proteoglycan, TNFα-stimulated gene-6 (TSG-6), is active in the brain from birth onward and differentially modifies ECM HA during discrete neurodevelopmental windows. ECM HA modification by TSG-6 enables it to serve as a developmental switch to regulate the activity of the Hippo pathway effector protein, yes-associated protein 1 (YAP1), in the maturing brain and in response to H–I injury. Mice that lack TSG-6 expression display dysregulated expression of YAP1 targets, excitatory amino acid transporter 1 (EAAT1; glutamate–aspartate transporter) and 2 (EAAT2; glutamate transporter-1). Dysregulation of YAP1 activation in TSG-6$^{-/-}$ mice coincides with age- and sex-dependent sensitization of the brain to H–I injury such that 1-week-old neonates display an anti-inflammatory response in contrast to an enhanced proinflammatory injury reaction in 3-month-old adult males but not females. Our findings thus support that a key regulator of age- and sex-dependent H–I injury response in the mouse brain is modulation of the Hippo-YAP1 pathway by TSG-6–dependent ECM modifications.

Key words: extracellular matrix; hypoxic–ischemic injury; link-domain proteoglycan; neonatal brain injury; signal transduction

Significance Statement

Hypoxic–ischemic (H–I) injury is a common cause of morbidity and mortality worldwide. Numerous genomic and proteomic screens have identified changes in the extracellular matrix (ECM) as the most common finding, yet the downstream mechanistic insights remain obscure. We found that proteoglycan TNFα-stimulated gene-6 (TSG-6)-dependent ECM modifications regulate the activity of the Hippo pathway effector, the RNA transcription coactivator, yes-associated protein 1 (YAP1). Dysregulation of YAP1 activation in TSG-6$^{-/-}$ mice coincided with age- and sex-dependent sensitization of the brain to H–I injury such that neonates displayed an anti-inflammatory response in contrast to an enhanced proinflammatory injury reaction in adults. Thus, our findings establish TSG-6–dependent ECM modifications as a key regulator of age- and sex-dependent H–I injury responses.

Received Nov. 28, 2023; revised March 24, 2024; accepted March 27, 2024.

Author contributions: T.S., S.B., and S.A.B. designed research; T.S., H.N., G.H., P.D., S.S., N.L., W.R-D., W.Z., and X.G. performed research; E.N.H. contributed unpublished reagents/analytic tools; T.S., H.N., G.H., P.D., S.S., N.L., and S.B. analyzed data; T.S. wrote the paper.

This project was supported by National Institute of Neurological Disorders and Stroke (NINDS) R01 NS116674 (S.A.B.) and R01 GM147913 (E.N.H.). T.S. was supported by a Huebner family career development fellowship. We thank Drs. Paul A Rosenberg and Manideep Chavali for their critical comments regarding this manuscript.

The authors declare no competing financial interests.

Correspondence should be addressed to Taasin Srivastava at srivasta@ohsu.edu or Stephen A. Back at backs@ohsu.edu.

https://doi.org/10.1523/JNEUROSCI.2215-23.2024

Introduction

Hypoxic–ischemic (H–I) brain injury is a common cause of morbidity and mortality throughout life. Cerebral palsy is the major complication in newborn infants who sustain hypoxic–ischemic encephalopathy (HIE; Ferriero, 2004; Millar et al., 2017). Globally, one in four adults over the age of 25 will also have a stroke in their lifetime (Feigin et al., 2022). Despite the high incidence of chronic neurological sequelae from H–I, regenerative therapies are needed that harness endogenous signaling or gene expression pathways. Changes in the brain extracellular matrix

(ECM) commonly occur in association with inflammatory and regenerative responses to H–I, but the mechanisms that may be exploited for tissue/cell repair remain obscure. Modifications of the brain ECM have received little attention as a regulator of H–I injury responses. In the brain, the main component of the ECM is the glycosaminoglycan hyaluronic acid (HA). In response to some forms of CNS injury, HA can transiently depolymerize and then reaccumulate to negatively influence regeneration pathways (Back et al., 2005; Srivastava et al., 2018).

Under homeostatic conditions, proteoglycan–HA complexes maintain the integrity and support the function of the ECM. This interaction between the large aggregating chondroitin sulfate proteoglycans (CSPGs) and HA is dependent on proteins, which contain link domains (Spicer et al., 2003). Unlike the hyaluronan and proteoglycan link protein family, which contains two link domains, TNFα-stimulated gene-6 (TSG-6) contains only one, which confers unique HA-binding properties (Spicer et al., 2003; Bano et al., 2018; Day and Milner, 2019). Apart from its link-domain–related function, TSG-6 can alter ECM rigidity by directly cross-linking HA (Milner and Day, 2003; Baranova et al., 2011). In the brain, oligodendrocytes are the main cell type regulating tissue stiffness and constitutive expression of several ECM components including TSG-6 (Tabula Muris Consortium et al., 2018; Segel et al., 2019; Kohnke et al., 2021; Elbaz et al., 2024). The ECM HA cross-linking property of TSG-6 is impaired by inter-α-inhibitor (IαI), a serum CSPG (Baranova et al., 2013). In the presence of IαI, a stochastic transesterification reaction exchanges TSG-6 in the ECM with the IαI-"heavy chain" (HC) subunits, which effectively blocks TSG-6-dependent HA cross-linking (Baranova et al., 2013). IαI is composed of three different gene products, *Itih1*, *Itih2*, or *Itih3*, coding for the HC 1, 2, or 3 subunits, which together with *Ambp* is assembled around a chondroitin-4-sulfate (C4S) backbone (Salier et al., 1996). Even though the *Itih1-4* genes can be detected in almost all tissues, IαI is assembled primarily in the liver for secretion into the serum as *Ambp* expression is liver-restricted (Salier et al., 1996).

Interestingly, TSG-6 has been shown to exert potent neuroprotection in models of stroke and inflammation (Bertling et al., 2016; Cui et al., 2023; Di Santo et al., 2023), but the underlying mechanisms are unclear. Since an anti-inflammatory role for TSG-6 in neonatal HIE was undefined, we employed TSG-6$^{-/-}$ mice to investigate whether it can also promote protection in neonates. Although we demonstrate here that stroke lesions are enhanced in TSG-6$^{-/-}$ adult mice (Cui et al., 2023; Di Santo et al., 2023) paradoxically, we found that deletion of TSG-6 was protective against H–I in neonates. We demonstrate that TSG-6–dependent ECM modification is regulated during discrete neurodevelopmental windows, which modulates the differential inflammatory responses to H–I in neonates and adults. We identify that these differential responses to H–I injury in TSG-6$^{-/-}$ neonates versus adults are dependent on the homeostatic regulation of yes-associated protein 1 (YAP1) activity. Mice that do not express TSG-6 show dysregulated activation of the Hippo pathway effector, YAP1, an RNA transcription coactivator, linked with regulation of metabolism and expression of amino acid transporters (Ma et al., 2019; Ibar and Irvine, 2020). Dysregulation of YAP1 activation in neonatal and adult TSG-6$^{-/-}$ brains coincides with maturation-dependent sensitization to H–I injury. Transcriptomic analysis by RNA-sequencing (RNA-seq) supports that disruption of TSG-6–dependent ECM modification predisposes the neonatal brain to a proinflammatory response. Our findings thus support that a key regulator of age- and sex-dependent H–I injury responses in the mouse brain is modulation of Hippo-YAP1 actions by TSG-6–dependent ECM modifications.

Materials and Methods

Animals. TSG-6$^{-/-}$ mice backcrossed into the C57Bl/6J background were a kind gift from Dr. Mark Aronica, Lerner Research Institute. WT C57BL/6J mice were from the Jackson Laboratory. The experimental neonatal and adult TSG-6$^{+/+}$ and TSG-6$^{-/-}$ animals used were generated by crossing either TSG-6$^{+/-}$ into TSG-6$^{+/-}$ or TSG-6$^{+/-}$ male or female mice. The TSG-6$^{+/+}$ and TSG-6$^{+/-}$ mice generated from the crosses served as litter-matched controls for all experimental studies unless otherwise indicated. Colony room conditions were maintained at 18–23°C and 40–60% humidity. All experimental procedures using animals were approved by the Institutional Animal Care and Use Committee at Oregon Health and Science University (OHSU; Protocol No. IP00000837). For all the experiments involving neonatal animals including forebrain slice cultures and H–I injury model, mixed numbers of male and female mice were used. For all the other experiments, male and female mice were used in equal proportions. The genotype, age, and numbers of mice used for each experiment are detailed in the figure legends. Genotypes for all animals were confirmed by conventional PCR analysis.

Neonatal H–I procedure. We employed a neonatal H–I injury protocol for Postnatal Day 7 (P7; 1-week-old) mouse pups exposed to 30 min of 8% hypoxia postsurgery (Lodygensky et al., 2011) as previously adapted from the Vannucci model (Vannucci and Back, 2022). Neonatal P6–7 mouse pups (male and female; 3.75–4.5 g) were employed for the H–I experiments. A total of 48 animals from eight different litters were used for the H–I procedure out of which 38 pups survived both surgery and hypoxia exposure (mortality rate 21%). Neonatal animals survived 72 h post H–I, and the dissected brains were immersion fixed in 4% paraformaldehyde (PFA) instead of perfusion due to the small body size of P9–10 mouse pups. After 48 h of fixation, the whole brains were rinsed three times with 1× PBS and then scored for injury. Only brains with grossly visible swelling in the ipsilateral hemisphere compared with the contralateral (uninjured hemisphere; 30 out of 38) were analyzed by immunohistochemistry (IHC). From this cohort of injured pups, we employed 10 TSG-6$^{+/+}$ (seven male and three female) and 8 TSG-6$^{-/-}$ (six male and two female) pups. Investigators were blinded to genotype identities during experimental procedures, which were confirmed only after the initial analysis was complete.

Adult middle cerebral artery occlusion (MCAO) procedure. Transient focal cerebral ischemia was induced in 3-month-old (P90) adult TSG-6$^{+/+}$ and TSG-6$^{-/-}$ male and female C57Bl/6J mice (20–26 g; $n = 10$ sex/genotype) using the intraluminal MCAO technique as described previously (Zhu et al., 2014). This model was employed in preference to an adult version of the Rice–Vannucci model because adult rodents subjected to unilateral carotid ligation are resistant to injury from hypoxia and the Levine model is too severe to observe graded cerebral injury resembling stroke (Vannucci and Back, 2022). Briefly, mice were anesthetized with isoflurane (5% for induction and 1.2–1.5% for maintenance in O_2-enriched air by face mask) and kept warm with water pads. A small laser Doppler probe was affixed to the skull to monitor ipsilateral cortical perfusion and verify vascular occlusion and reperfusion. A silicone-coated 7-0 nylon monofilament (Doccol) with silicone-coated tip (0.20 ± 0.01 mm diameter) was inserted into the right internal carotid artery via the external carotid artery until the laser Doppler signal dropped to <30% of the baseline. The filament was withdrawn to allow for reperfusion at 60 min occlusion. Mice were then allowed to recover under observation. Infarct size was measured at 24 h after MCAO in 2-mm-thick coronal brain sections (four in total) using 2,3,5-triphenlytetrazoilum chloride (TTC) staining and digital image analysis. Sections were incubated in 1.2% TTC in saline for 15 min at 37°C and then fixed in formalin for 24 h. Slices were photographed, and infarcted (unstained) and

uninfarcted (red color) areas were measured with ImageJ and integrated across all four slices. To account for the effect of edema, we estimated the infarcted area indirectly by subtracting the uninfarcted area in the ipsilateral hemisphere from the contralateral hemisphere and expressing infarct volume as a percentage of contralateral hemisphere. Investigators were blinded to genotype identities during experimental procedures, which were confirmed only after the initial analysis was complete.

Pharmacological reagents. Recombinant human TSG-6 (rhTSG-6; catalog #2104-TS; R&D Systems); recombinant human Wnt3a (catalog #5036-WN; R&D Systems); 2,3,5-triphenyltetrazolium chloride (catalog #T887; Sigma-Aldrich); *Streptomyces* hyaluronidase (catalog #389561; MilliporeSigma)

IαI purification. The IαI complex was extracted from the commercially available human serum. Briefly, human serum was subjected to diethylaminoethyl resin, and then the eluted material was separated by a Superose 6 10/300 size-exclusion chromatography column on an Agilent 1100. We obtained four protein peaks from the elution, and the second peak at 30 min was identified as IαI by mass spectrometry. Protein concentrations were determined by UV measurements, and to ensure peak activity, we performed the experiments involving the IαI complex purified from the human serum within 48–72 h following extraction. Purified serum IαI complex has been observed to have compromised stability if stored as it tends to aggregate and partly degrade over time (Enghild et al., 1989).

Hyaluronidase assays and Western blotting. For performing protein analysis, brains of different aged pups and animals were extracted; the cortex was microdissected and immediately frozen in liquid nitrogen (LN_2) and stored at −80°C until all the samples for a particular experimental analysis were collected. After collection, to avoid batch effects, we prepared the protein lysates from all the samples on the same day and processed them for concentration quantification. Protein concentrations were estimated by the standard BCA assay (Thermo Fisher Scientific), and 35 µg of total protein lysate was employed for all downstream Western blotting analysis and assays. To verify whether HA was modified by IαI-HC, and/or to determine the status of Hippo-YAP signaling in TSG-$6^{+/+}$, TSG-$6^{+/-}$, and TSG-$6^{-/-}$ brains, we prepared the protein lysates using the NE-PER buffer (Thermo Fisher Scientific) supplemented with protease and phosphatase inhibitors from either the previously microdissected and frozen cortical tissue blocks or the cultured forebrain slices. For hyaluronidase assays, 35 µg of protein lysates prepared from different ages and conditions (as indicated in figure legends) were treated with either *Streptomyces* hyaluronidase (Tocris Bioscience; 1 U/ml) or PBS, immediately transferred to a water bath maintained at 37°C and incubated for 60 s. Following incubation, the enzyme activity was quenched by directly adding the SDS loading buffer to the lysates and boiling. All protein lysates were subjected to SDS-PAGE using 4–20% gels (Bio-Rad Laboratories and Invitrogen) and blotted onto Immobilon-FL PVDF membrane (MilliporeSigma). The following antibodies were used: WWTR1 [tazzafin (TAZ); 1:1000 catalog #HPA007415; Sigma-Aldrich], TSG-6 (1:500; clone 259820; catalog #MAB2104; R&D Systems), pYAP1-Y357 (1:500; catalog #ab62751; Abcam), and IαI (1:2000; catalog #A0301; Dako); glutamate transporter-1 (GLT-1; 1:3000; catalog #PA5-80011), glutamate–aspartate transporter (GLAST; 1:500; PA5-72895), and Cx30 (1:1000; clone Z-PP9; catalog #71-2200) which were all purchased from Thermo Fisher Scientific; and actin (1:5000; catalog #3700), pYAP1-S127 (1:1000; catalog #4911), Mst1 (1:1000; catalog #3682), pLATS1-S909 (1:1000; catalog #9157), NF2 (1:1000; clone D353W; catalog #12888), LATS2 (1:1000; clone D8306; catalog #5888), and LATS1 (1:1000; clone C66B5; catalog #3477) which were purchased from Cell Signaling Technology. The secondary IR680 and IR800 antibodies were purchased from Rockland Immunochemicals and used at 1:20,000. To quantify changes in IαI-HC signal intensity from the lysates subjected to heparinase (H'ase) or PBS treatment, we normalized the values to total HC3 protein detected by the IαI antibody as previously described (Fasanello et al., 2021). To quantify changes in signal intensities for all the other proteins, we normalized the densitometry values to actin. Densitometry values were obtained via Image Studio Lite (LI-COR Biosciences).

Forebrain slice culture. To assay serum- and IαI-mediated HA remodeling, we prepared forebrain slice cultures utilizing neonatal P4–5 mouse pups. Serially matched 350-µm-thick sections were cut using the vibratome from live brains and plated onto cell culture inserts (0.45 µm pore size; MilliporeSigma) containing either DMEM supplemented with 5% horse serum (HS) or artificial cerebrospinal fluid (containing the following in mM: 125 NaCl, 2.5 KCl, 2 $CaCl_2$, 1 $MgCl_2$, 5 HEPES, and 33 glucose; pH 7.3; 290–300 Osm) supplemented with or without purified IαI (400 ng/ml). The slices were treated for the times indicated in the figure legends, following which they were either lysed in the NE-PER buffer (Thermo Fisher Scientific) supplemented with protease and phosphatase inhibitors to prepare protein lysates for hyaluronidase assay and Western blotting or fixed with ice-cold 4% PFA for IHC analysis or processed to extract RNA (Qiagen) for bulk RNA-seq analysis. All the slices were cultured without the presence of antibiotics.

IHC. The following antibodies were used in this study: component 3a receptor (C3aR; 1:500; clone 14D4; catalog #HM1123; Hycult Biotech); glial fibrillary acidic protein (GFAP; 1:500; catalog #MAB360; MilliporeSigma); ionized calcium-binding adapter molecule 1 (Iba1; 1:500; catalog #019-19741; Wako Pure Chemical Industries); and neuronal nuclei (NeuN; 1:500; MAB377; MilliporeSigma). Nuclei were counterstained with DAPI (Invitrogen). Antigen retrieval was employed for all antibodies (0.01 M citrate buffer, pH 6.0, 85°C, 15 min). All corresponding secondary antibodies were from Jackson ImmunoResearch Laboratories. No primary control studies for all antibodies exhibited no specific staining.

Plasmids, transfection, and luciferase assay. The YAP-TEAD luciferase reporter 8xGTIIC plasmid was obtained from Addgene (Dupont et al., 2011). The CMV-*Renilla*-LUC was obtained from Promega. The HEK293A cells were a kind gift from Dr. Monika Davare (Department of Pediatrics, OHSU). For a typical luciferase assay, the 293A cells were plated at a density of 60,000 cells/well in 24-well plates supplemented with DMEM containing 5% FBS. Six hours after plating, the 8xGTIIC-Luc and CMV-*Renilla* luciferase reporter plasmids were cotransfected using Lipofectamine 2000 (Invitrogen) as per manufacturer instructions. Ten to twelve hours following transfection, the cells are transferred to 0.1% serum containing media for 4–6 h (serum starvation) after which the cells were either stimulated with DMEM containing 5% serum and supplemented with or without recombinant human TSG-6 (rhTSG-6; 200 ng/ml; R&D Systems) or treated with rhTSG-6 (200 ng/ml) or Wnt3a (100 ng/ml; Tocris Bioscience) in the 0.1% serum containing DMEM. Twelve hours after treatment, the transfected cells were lysed, and luciferase activity was assayed with the Dual-Glo Luciferase Assay System (Promega) following manufacturer instructions. Firefly luciferase activity was normalized to *Renilla* luciferase activity. All assays were done in triplicate, and the experiment was repeated three separate times.

Real-time PCR. Brains from different aged animals (as indicated in figure legends) were harvested, microdissected to extract the cortex, immediately frozen in LN_2, and stored at −80°C. A small frozen tissue piece was chipped from the frozen cortex and then used to prepare total RNA using the RNeasy Tissue Kit (Qiagen). Two hundred fifty nanogram of RNA was used to prepare cDNA library using the Taqman Reverse Transcription Kit (Applied Biosystems). cDNA was diluted 1:1 before real-time PCR (qPCR) experiments (Taqman Gene Expression Master Mix, Applied Biosystems). All qPCR probes were FAM-MGB: *Tnfaip6* (Mm00493736_m1) and 18S (Rn03928990-g1). The 18S rRNA was used as the endogenous control for all time points. Ct values were used to calculate fold change [$2^{-(\Delta\Delta Ct)}$] in gene expression normalized to the 18S control for each age. The fold change is calculated based on two independent experiments where Ct values were averaged from three technical replicates per experiment.

Bulk RNA-seq and bioinformatic analysis. Total RNA was extracted from the cultured forebrain slices and stored in diethylpyrocarbonate-treated water using the RNeasy Micro Kit (Qiagen). The quality and quantity of extracted RNA were assessed using the Agilent 2100 BioAnalyzer RNA 6000 Pico Chip with each sample averaging ~200 ng of RNA and all samples having an RNA integrity number of >9. We prepared cDNA libraries using the SMART-Seq v4 chemistry (Takara Bio) and sequenced the libraries on an HiSeq 2500 (Illumina). TopHat2 with default parameters was used to align the sequenced reads against the mouse genome using the GRCm38. HTSeq Python software with default parameters was used to quantify the transcripts of the aligned reads using the corresponding GRCm38 gene annotation model from Ensembl, and the downstream analysis was done in RStudio (v.2023.03.0 + 386). Raw read counts were processed and normalized using the median of ratio method. Low-abundance genes below a mean count of 5 reads per sample were filtered out. The normalized counts were then used to perform principal component analysis (PCA) in RStudio, which confirmed that serum treatment leads to differential responses from TSG-6$^{+/+}$ and TSG-6$^{-/-}$ forebrain slice cultures. The count data was used as an input for differentially expressed gene (DEG) analysis using DESeq2 (v.1.38.3; R package; Love et al., 2014), which identified differentially expressed genes between the genotypes after serum treatment by running comparisons using the likelihood ratio test where the cutoff for significant genes was a Benjamin–Hochberg FDR-corrected $p < 0.05$ (Tables 2-5, 6-2). The volcano plot displaying the log2 fold changes (−1.5 to +1.5) between the genotypes was visualized using EnhancedVolcano (v1.16.0; R package). The normalized gene counts were also used as an input for gene set enrichment analysis (GSEA; Subramanian et al., 2005) to identify cellular pathways dysregulated between the genotypes.

Cell counts. These were performed using the Fiji cell counter plugin (ImageJ, NIH) on brain sections from TSG-6$^{+/+}$ and TSG-6$^{-/-}$ neonatal and adult brains. The infarct and peri-infarct areas in adult and neonatal mice were defined based on differential GFAP, Iba1, and DAPI staining. In adult brains, the infarct area typically spanned across all the cortical layers and displayed shrunken and/or no nuclei as identified by DAPI and virtually no and/or very minimal GFAP and Iba1 staining. In contrast, the brain tissue immediately adjacent to infarct displayed morphologically transformed cells expressing high levels of GFAP and Iba1, which progressively decreased in intensity as the distance from the border increased. This adjacent region displaying transformed GFAP$^+$ and Iba1$^+$ cells was designated as the peri-infarct area. For both the genotypes, one adjacent brain section was also stained with NeuN antibody to confirm the location of the infarct border as NeuN$^+$ cells could be found in the peri-infarct but not the infarct region. For scoring Iba1$^+$ and C3aR$^+$ cells in the peri-infarct area, a 350-µm-wide rectangular region of interest (ROI) extending from the edge of the infarct and encompassing the entire cortical layers was analyzed. Unlike the adults, in the neonates, discerning the exact boundary of infarct and peri-infarct was difficult due to the small size of the lesions; therefore, the injured areas were defined by the presence of morphologically transformed cells expressing GFAP and Iba1 as well as shrunken nuclei labeled by DAPI. For scoring Iba1$^+$ and C3aR$^+$ cells, a 400 × 400 µm ROI encompassing the tissue area displaying high GFAP signal was analyzed. For adults, 2 sections/animal/genotype whereas for neonates 1–2 sections/animal/genotype were analyzed.

Astrocyte morphology analysis. We determined the magnitude of hypertrophy of GFAP-labeled astrocytes in brain sections from TSG-6$^{+/+}$ and TSG-6$^{-/-}$ neonatal and adult brains as well as forebrain slice cultures. The imaging of GFAP$^+$ cells (*z* stacks) was performed with a laser scanning confocal microscope (LSM700, Zeiss,) using the ZEN software. *Z* stacks images were processed in Fiji (ImageJ, NIH) to generate maximum-intensity projection images, which were flattened for analysis. For the analysis of hypertrophic cells in each neonatal H–I lesion, a 400 × 400 µm ROI was analyzed. In adult lesions, a 300 µm-wide rectangular ROI extended from the edge of the lesion and encompassed cortical layers (II–VI) defined by DAPI staining. For forebrain slice cultures, cortical GFAP-labeled cells were selected for analysis by drawing a 400 × 400 µm ROI. To ensure consistency, the same ROI was selected for comparison between genotypes. The branches of GFAP$^+$ cells were traced with the simple neurite tracer plugin using Fiji. The thickness of individual processes was estimated at 15 µm from the soma. Three-dimensional Sholl's analysis was performed with soma of the stained cell serving as the center. The starting circle's radius was set at 5 µm, and each step distance was 5 µm. Twenty to forty GFAP$^+$ cells were randomly selected and assessed per ROI. A total of eight sections/genotype (neonates), six sections/genotype (adults), and nine sections/genotype (slice cultures) were analyzed.

Confocal analysis. All confocal imaging was performed on an inverted Zeiss LSM700 microscope using either the 10× or 20× air objectives. The data were collected using the Zeiss ZEN software. Images of either 1,024 × 1,024 or 2,048 × 2,048 pixels with a *z* interval of 3 µm were collected. Gain and offset were set at values that prevented saturated and empty pixels. The laser setting was kept the same between the genotypes for the set of images collected per session/experiment. All image processing was done while blinded to the mouse genotype in Fiji.

Experimental design and statistics. Our sample sizes for the neonatal and adult H–I studies were decided by a power analysis based on our preliminary and previous results using a two-sided α 0.05 and β 0.2. Statistical analysis was performed using the Prism 10.1 statistical software (GraphPad Software). For all comparisons between two groups, the comparisons were made by either unpaired or paired two-tailed Student's *t* test. If the data were not normally distributed, two-tailed Welch's correction test for comparisons was used to examine the differences between the two groups. One-way or two-way ANOVA tests were used to determine statistical significance for more than two groups. After observing a significant effect of treatment, a post hoc analysis by Sidak's or Tukey's test was done to determine differences between the groups, and $p < 0.05$ was considered statistically significant. Data are presented as the mean ± SEM. Data for each experiment were collected and processed randomly; animals were assigned to various experimental groups randomly. All *n* and *p* values and statistical tests are indicated in figure legends.

Results

TSG-6 confers sex-dependent protection in an in vivo model of adult stroke injury

Pretreatment with recombinant TSG-6 has been proposed to provide protection from experimental stroke injury induced by MCAO, but those studies either did not consider or were not sufficiently powered to detect sex differences (Cui et al., 2023; Di Santo et al., 2023). Sex is a key risk factor that influences ischemic stroke susceptibility with younger males generally being more vulnerable than females (Roy-O'Reilly and McCullough, 2018). We sought to determine whether the proposed TSG-6–mediated protection from ischemic injury could be sex-dependent.

To test this, we subjected TSG-6$^{+/+}$ and TSG-6$^{-/-}$ sex- and age-matched young adult mice to a MCAO procedure, which subjected one hemisphere to H–I. We collected tissue samples at 24 h after H–I to define the role of TSG-6 in regulating lesion infarct size volumes. Changes in infarct size volumes were analyzed by 2,3,5-TTC staining, which detects intact mitochondrial activity in living versus dead tissue (Bederson et al., 1986). H–I led to reduced TTC staining in the tissue derived from both sexes and genotypes, but surprisingly, TSG-6$^{-/-}$ males displayed a significant increase in total infarct volumes in the cortex and hemisphere when compared with TSG-6$^{+/+}$ males (Fig. 1*A*,*B*). In contrast, we found no significant differences in total lesion infarct volumes in the cortex or hemisphere of TSG-6$^{+/+}$ and TSG-6$^{-/-}$ female mice (Fig. 1*A*,*B*). No differences in the total

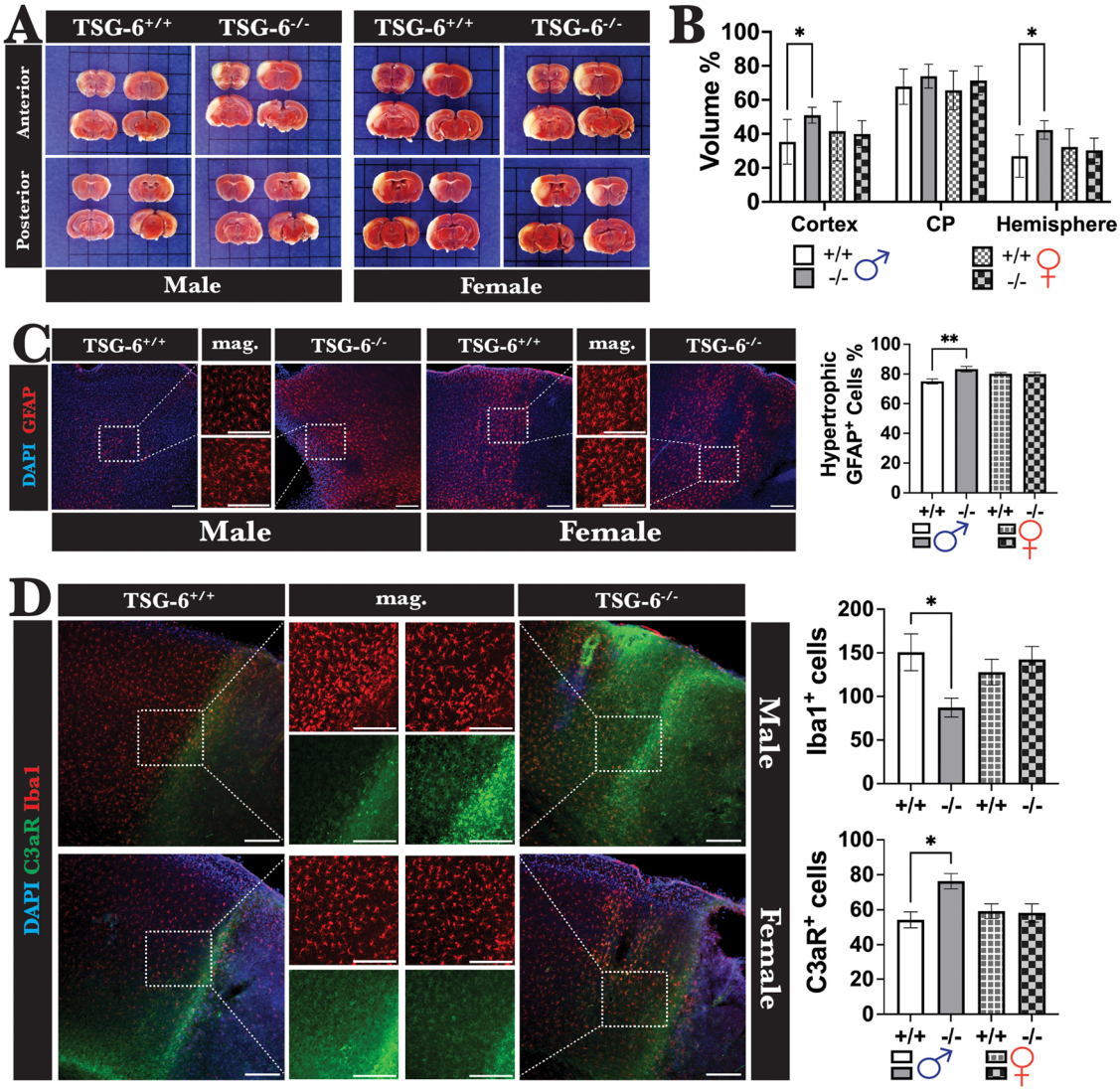

Figure 1. TSG-6 confers sex-dependent protection in an in vivo model of adult stroke injury. ***A***, Twenty-four hours postinjury, the ischemic lesions defined by loss of TTC staining are larger in male TSG-6$^{-/-}$ brains compared with TSG-6$^{+/+}$. In contrast, comparable level of ischemic injury is observed in female TSG-6$^{+/+}$ and TSG-6$^{-/-}$ brains. Representative anterior and posterior brain slices depicting ischemic lesions in both genotypes and sexes. ***B***, Quantification of changes in lesion volumes in the cerebral cortex, CP, and whole hemisphere between the male and female genotypes. ***C***, Significant upregulation of hypertrophic GFAP-expressing cells 72 h after injury observed in male TSG-6$^{-/-}$ lesions compared with TSG-6$^{+/+}$ but no striking morphological differences noted in the GFAP^{+} cells found in female ischemic injury lesions of both the genotypes. Magnification (mag.) of the leading edge of the ischemic lesions. Quantification of total percentage of hypertrophic GFAP^{+} cells in ischemic lesions of male and female genotypes. ***D***, A decrease in the number of Iba1^{+} and an increase in C3aR^{+} cells are observed at the leading edges in male TSG-6$^{-/-}$ ischemic injury lesions compared with TSG-6$^{+/+}$. Similar numbers of Iba1^{+} and C3aR^{+} cells are observed in the female TSG-6$^{+/+}$ and TSG-6$^{-/-}$ ischemic injury lesions. The quantification of Iba1^{+} and C3aR^{+} cells reveals significant differences in the male but not female genotypes. $n = 7$ animals/genotype/sex (***A,B***); $n = 3$ animals/genotype/sex (***C,D***); *$p < 0.05$ by two-way ANOVA (***B***); *$p < 0.05$ and **$p < 0.01$ by one-way ANOVA (***C,D***); error bars indicate ±SEM. Scale bars: 300 µm (***C,D***), 75 µm (***C***), and 100 µm (***D***) for magnifications.

infarct volumes in the caudate putamen (CP) were noted for either sex (Fig. 1*B*). Hence, TSG-6 exerts a protective role in adult ischemic injury that is sex-dependent.

Upregulation of glial inflammatory states is a hallmark of ischemic injury. Given that TSG-6$^{-/-}$ males were particularly sensitive to H–I, we examined changes in astrocyte (GFAP) and microglial (Iba1) reactivity at 72 h postinjury. We found a robust GFAP response to H–I injury across the genotypes and sexes, but the most pronounced differences were found between the TSG-6$^{+/+}$ and TSG-6$^{-/-}$ males where the total percentage of GFAP^{+} cells displaying hypertrophy was significantly increased, whereas no changes in females were noted (Fig. 1*C*).

Following ischemic injury, Iba1^{+} microglia initiate inflammatory responses that depend on complement signaling cues from reactive astrocytes (Liddelow and Barres, 2017) but can also promote repair by rapidly expanding, which aids in attenuating the size of ischemic infarct volumes (Lalancette-Hebert et al., 2007). Secretion of complement protein C1q by reactive GFAP^{+} cells induces cleavage of C3 to generate C3a and C3b fragments (Gasque, 2004). The local Iba1^{+} microglia respond to C3 fragments and upregulate specific complement-induced C3 receptor (C3R) expression, which further exacerbates oxidative stress and inflammation (Liddelow and Barres, 2017). Consistent with the hypertrophic astrocyte responses in males versus females, we found higher numbers of C3aR-expressing cells in the infarct and peri-infarct areas in the TSG-6$^{-/-}$ but not TSG-6$^{+/+}$ males (Fig. 1*D*). Moreover, we found a significant reduction in the density of Iba1^{+} microglial cells in the infarct and peri-infarct areas in the TSG-6$^{-/-}$ but not TSG-6$^{+/+}$ males (Fig. 1*D*). We also found that the alterations were limited to

only TSG-6$^{-/-}$ males as analysis of infarct and peri-infarct lesion areas in TSG-6$^{-/-}$ female brains revealed nonsignificant changes in C3aR^{+} and Iba1^{+} cells compared with TSG-6$^{+/+}$ females (Fig. 1*D*). Taken together, our findings support that TSG-6 plays a key role in regulating sex-dependent adult inflammatory glial responses to ischemic injury.

TSG-6 promotes proinflammatory injury in an in vivo model of neonatal H–I

Given the potent sex-dependent neuroprotection mediated by TSG-6 in response to adult H–I, we determined whether TSG-6 can also promote anti-inflammatory states in the neonatal brain following ischemic injury in vivo. After we induced H–I in wild-type neonatal mouse pups (see Materials and Methods, Neonatal H–I procedure), we examined the extent of injury in the cerebral cortex by analyzing changes in GFAP expression and serum albumin accumulation, which were confined to the ipsilateral (injured) hemisphere (data not shown).

We next induced H–I in TSG-6$^{+/+}$ and TSG-6$^{-/-}$ pups. In contrast to the adult TSG-6$^{-/-}$ response to H–I, hypertrophic GFAP^{+} astrocyte responses to injury were markedly reduced in the TSG-6$^{-/-}$ neonatal mice (Fig. 2*A*,*B*). Few hypertrophic astrocytes were observed in the core of TSG-6$^{-/-}$ H–I lesions. Rather, most astrocytes displayed palisading cell processes, which aligned with the pial surface and appeared to form a boundary around the injury site (Fig. 2*A*, white arrows). No boundary-forming palisading astrocytes were observed in TSG-6$^{+/+}$ lesions, where the core was instead dominated by hypertrophic reactive astrocytes (Fig. 2*A*). Since palisading astrocytes have been proposed to be involved in repair and neuroprotection by promoting anti-inflammatory pathways (Faulkner et al., 2004), we determined whether the lesions in TSG-6$^{-/-}$ brains were associated with an altered inflammatory microenvironment. We first analyzed the expression of nuclear factor erythroid 2-related factor 2 (Nrf2), a transcription factor that functions to limit oxidative stress and inflammation (Ma, 2013). Nrf2 expression was markedly diminished in regions populated by hypertrophic astrocytes associated with the core of TSG-6$^{+/+}$ H–I lesions (Fig. 2*A*). In contrast, Nrf2 expression was markedly upregulated in the TSG-6$^{-/-}$ H–I lesions (Fig. 2*A*) suggesting that the TSG-6$^{-/-}$ lesion microenvironment may be more conducive for repair processes.

C3aR has emerged as a therapeutic target for neonatal H–I (Jarlestedt et al., 2013). C3aR expression by microglia as well as neurons (Davoust et al., 1999) is required for the recruitment of peripheral cells into the brain parenchyma (Wu et al., 2016) and regulates microglial phagocytosis (Lian et al., 2016). Antagonizing C3aR activation in the acute phase of ischemic injury in neonates promotes outcomes favoring regeneration and repair (Jarlestedt et al., 2013). We found a significant increase in the number of Iba1^{+} microglia in TSG-6$^{+/+}$ lesions typically associated with microglial activation (Fig. 2*A*,*B*). In contrast, activated Iba1^{+} microglia were not observed in the TSG-6$^{-/-}$ lesions (Fig. 2*A*, lower panel, white arrowheads, and 2*B*). Notably, the core of the TSG-6$^{+/+}$ lesions was populated with C3aR^{+} cells, whereas these cells were rarely detected in TSG-6$^{-/-}$ injured areas (Fig. 2*A*, lower panel, and 2*B*). Hence, in contrast to H–I injury in adult males, a lack of TSG-6 expression in neonates was associated with a phenotype exemplified by a lack of astrocyte reactivity or a microglial proinflammatory response.

To further test the hypothesis that TSG-6 promotes a proinjury state in neonates, we employed our in vitro model of neonatal brain injury (Srivastava et al., 2018) and examined changes in gene expression by unbiased bulk RNA-seq. We prepared forebrain slices from neonatal male and female TSG-6$^{+/-}$ and TSG-6$^{-/-}$ pups and exposed them to serum. After overnight culture, total RNA was extracted from the slices for bulk RNA-seq. We normalized the RNA counts and used the dimension reduction method, PCA, to determine whether the genotypes respond differently to the same serum treatment. The TSG-6$^{+/-}$ and TSG-6$^{-/-}$ samples displayed distinct differences between them (Fig. 2*C*, left panel). On the other hand, the response of male and female pups to serum did not differ (Fig. 2*C*, right panel). We next checked for sex differences, by analyzing the male and female samples separately. Surprisingly, the male brains displayed distinct genotype-dependent response to serum treatment (Fig. 2*D*, left panel), whereas no differences could be noted after the analysis of the female samples (Fig. 2*D*, right panel).

To determine whether the gene expression profiles of male and female TSG-6$^{+/-}$ and TSG-6$^{-/-}$ display enrichment of gene sets associated with specific biological pathways, we employed the GSEA (Subramanian et al., 2005). We queried the "Hallmark" gene set category of the Molecular Signature Database (MSigdb) for similarities in our normalized RNA counts dataset. We found that the top 10 Hallmark pathways activated in the TSG-6$^{+/-}$ male and female samples were mostly the same but were ranked differently. For example, the activation of the fatty acid metabolism and E2F pathways, involved in neurodegeneration and brain injury (MacManus et al., 2003; Bogie et al., 2020), was observed in both, but the normalized enrichment score (NES) differed (Fig. 2*E*; see Tables 2-1–2-2 for details). In contrast, the activation of the same gene set categories was observed in both TSG-6$^{-/-}$ male and female samples suggesting that they respond similarly to serum treatment (see Tables 2-3–2-4 for details). We next analyzed the male and female RNA-seq datasets for DEGs using the R package, DESeq2 (Love et al., 2014). Using this analysis and implementing a cutoff for significant genes with a Benjamin–Hochberg-adjusted $p < 0.05$, we were unable to identify any DEGs between the serum-treated neonatal female genotypes. On the other hand, we were able to identify 199 DEGs (Benjamin–Hochberg-adjusted $p < 0.05$) between the serum-treated neonatal male genotypes (Table 2-5).

Most of the DEGs were found in TSG-6$^{-/-}$, whereas relatively few genes changed in the RNA profile derived from TSG-6$^{+/-}$ brains (Fig. 2*F*). The genes upregulated in TSG-6$^{+/-}$ but not in TSG-6$^{-/-}$ males included *Fabp7*, a radial glia/astrocyte marker involved in reactive astrogliosis (Kipp et al., 2011; Sharifi et al., 2011; Killoy et al., 2020) and *Cx3Cr1*, a marker for activated microglial cells (Hickman et al., 2018), consistent with a proinjury state. Interestingly, the large HA-binding CSPGs *Bcan* and *Vcan* expressed by the astrocytes (Yamada et al., 1997) and oligodendrocytes (Asher et al., 2002), respectively, are also differentially expressed suggesting unique ECM HA modifications in the absence and presence of TSG-6 following injury (Fig. 2*F*). Neonatal oligodendrocytes respond to brain injury by undergoing expansion of premyelinating progenitors that are unable to mature leading to myelination failure (Back, 2017). Consistent with these observations, we found that *Bcas1*, a marker of premyelinating oligodendrocytes (Fard et al., 2017), and *Myef2*, a negative regulator of myelin basic protein expression in the developing brain (Haas et al., 1995), were upregulated in TSG-6$^{+/-}$ samples. In contrast, *Nf1*, which is involved in maintaining myelin integrity and keeping Ras MAPK activity in check

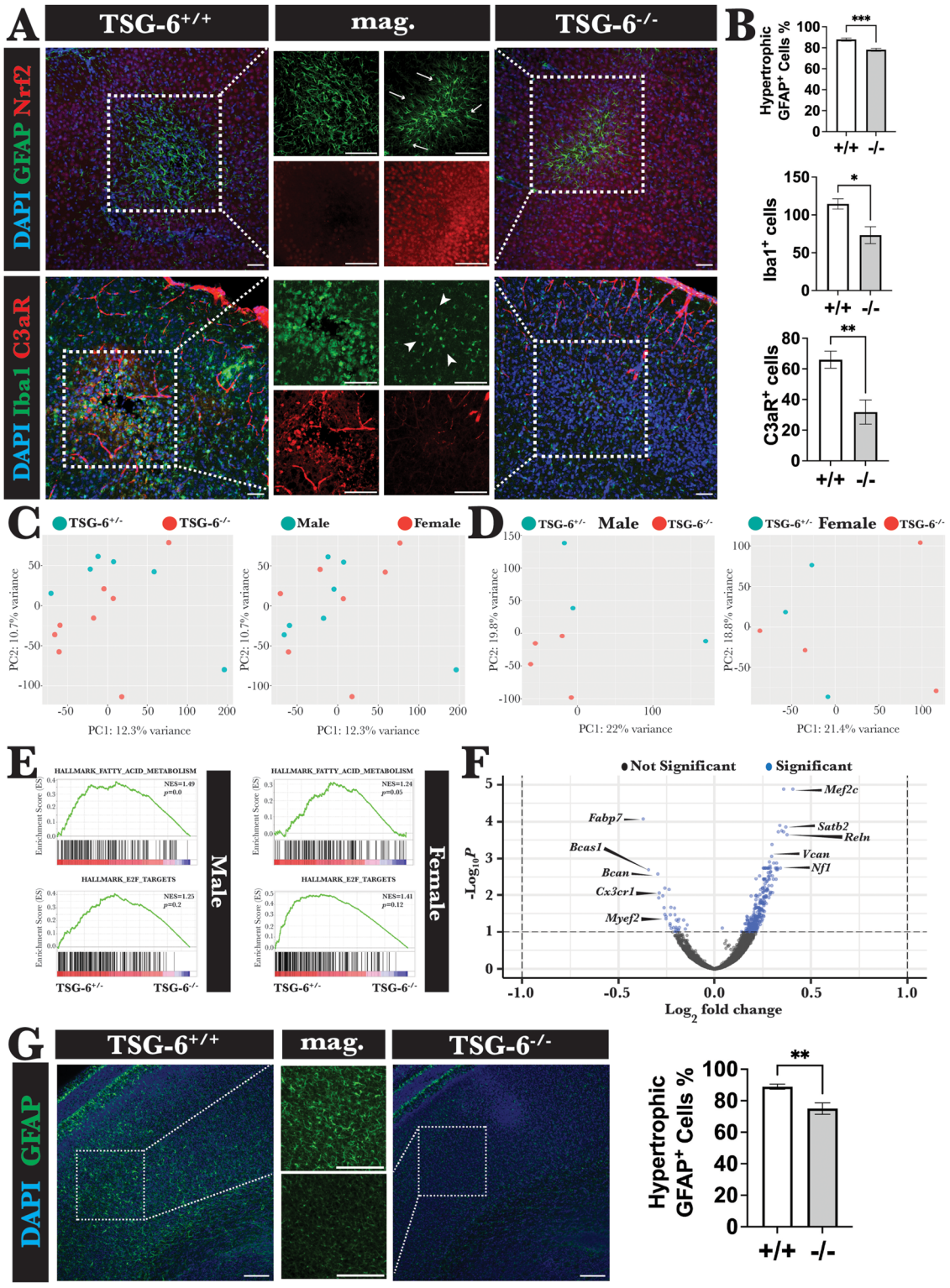

Figure 2. TSG-6 promotes proinflammatory injury in an in vivo model of neonatal H–I. ***A***, Top panels: 3 d postinjury, the ischemic lesions in neonatal (P10) TSG-6$^{+/+}$ brains lack palisading GFAP^{+} and Nrf2^{+} cells in comparison with their abundant presence in TSG-6$^{-/-}$ lesions. Bottom panels: The same lesion cores in TSG-6$^{+/+}$ brains are populated with Iba1^{+} microglial cells and C3aR cells compared with TSG-6$^{-/-}$. Magnifications of the ischemic lesion core (mag.). ***B***, Quantification of GFAP^{+} hypertrophic, Iba1^{+}, and C3aR^{+} cells found in the ischemic lesion core in both genotypes. ***C***, PCA of RNA-seq data shows the separation of TSG-6$^{+/-}$ and TSG-6$^{-/-}$ samples based on genotype (left panel) and but not sex (right panel). ***D***, PCA of only male and female RNA-seq data shows the separation of TSG-6$^{+/-}$ and TSG-6$^{-/-}$ neonatal males (left panel) but not females (right panel). ***E***, Representative GSEA plots showing the overrepresentation of Hallmark Fatty_Acid_Metabolism and E2F_Target gene sets among the DEGs for neonatal male and female TSG-6$^{+/-}$ and TSG-6$^{-/-}$ slice cultures treated with serum (see Tables 2-1–2-4 for details). NES and Kolmogorov–Smirnov test *p* values are indicated in graphs. ***F***, Volcano plot depicting the DEGs identified in serum-treated neonatal male TSG-6$^{-/-}$ slice cultures by DESeq2. Benjamin–Hochberg false discovery rate (FDR)-corrected $p < 0.05$ (see Table 2-5 for the complete list of DEGs and statistical details). ***G***, Serum treatment upregulates hypertrophic GFAP transformation in both TSG-6$^{+/+}$ (+/+) and TSG-6$^{-/-}$ (−/−) forebrain slice cultures, but the hypertrophy is significantly attenuated in −/− slice cultures (right panel). Magnifications of the serum-treated slice cultures (mag.). $n = 10$ TSG-6$^{+/+}$ (7 male and 3 female), $n = 8$ TSG-6$^{-/-}$ (6 male and 2 female) from eight separate experiments (***A***,***B***); $n = 3$/sex TSG-6$^{+/-}$ and $n = 4$/sex TSG-6$^{-/-}$ at P4 from four separate experiments (***C–F***); $n = 2$/genotype P4 male pups from two separate experiments (***G***). Error bars indicate ±SEM; ***$p < 0.001$, **$p < 0.01$, and *$p < 0.05$ by unpaired Student's *t* test with Welch's correction (***B***,***G***). Scale bars: 200 µm, 50 µm (mag., ***A***); 300 µm, 75 µm (mag., ***G***).

(Mayes et al., 2013), was upregulated in TSG-6$^{-/-}$ neonatal males. To further confirm that absence of TSG-6 leads to dysregulated glial reactivity, we stained serum-supplemented slice cultures prepared from TSG-6$^{+/+}$ and TSG-6$^{-/-}$ pups with GFAP. Consistent with the involvement of multiple transcription factor modules that regulate reactive astrogliosis (Lattke et al., 2021; Burda et al., 2022), we found GFAP^{+} cells in the forebrain slices from both the genotypes. However, when we analyzed cellular morphology of GFAP^{+} cells in the serum-treated slices from both genotypes, we found a small but significant reduction in the total percentage of hypertrophic cells from TSG-6$^{-/-}$ forebrain slice cultures (Fig. 2*G*). Taken together, these results suggest that TSG-6 paradoxically exerts a proinjurious state after neonatal injury, in contrast to a neuroprotective response in adult stroke.

TSG-6–dependent ECM HA modification is impaired during a discrete neonatal window

Although previous (Cui et al., 2023; Di Santo et al., 2023) and present findings suggest a role for TSG-6 in ischemic injury, the mechanisms remain poorly understood. TSG-6 is a link-domain–containing proteoglycan (Day and Milner, 2019). Link-domain–containing proteins typically maintain the integrity and function of the ECM by promoting the interaction between the large aggregating CSPGs and HA (Spicer et al., 2003). TSG-6's direct binding to HA itself promotes cross-linking and ECM rigidity (Baranova et al., 2011). Interestingly, the ECM-modifying properties of TSG-6 are impaired by IαI, a serum CSPG (Baranova et al., 2013). In the presence of IαI, a stochastic transesterification reaction exchanges TSG-6 out of the ECM and replaces it with the IαI-HC subunits effectively blocking TSG-6–dependent HA cross-linking (Fig. 3*A*). The IαI CSPG is enriched in serum as an evolutionary conserved component (Enghild et al., 1989; Sanggaard et al., 2010). H–I injury compromises the blood–brain barrier (BBB) and mediates the entry of serum proteins into the brain, which initiate inflammation (Carvey et al., 2009; Jiang et al., 2018). We thus hypothesized that H–I injury exposes the brain parenchyma to serum IαI which impairs TSG-6–dependent cross-linking while promoting IαI-HC modification of the ECM HA (Fig. 3*A*).

Due to differential response to H–I injury in neonate and adult TSG-6$^{-/-}$ animals, we first analyzed the expression of TSG-6 in the developing mouse brain as prior studies only focused on TSG expression in the adult rat (Coulson-Thomas et al., 2016). The analysis of RNA and protein brain lysates demonstrated that TSG-6 is constitutively expressed from birth to adulthood (Fig. 3*B*). To examine whether the IαI complex can disrupt TSG-6–dependent ECM HA cross-linking, we prepared forebrain slices from neonatal pups and exposed them to HS, which contains saturating amounts of IαI (Sanggaard et al., 2010). Following HS exposure (5%; 15 min), brain cortical protein lysates were briefly treated with *Streptomyces* hyaluronidase enzyme (1 U/ml; H'ase) or left untreated. H'ase treatment degrades ECM HA, which releases interacting HC proteins for downstream protein analysis (Lauer et al., 2015). Forebrain slice lysates subjected to H'ase digestion contained the "IαI-HC" subunit suggesting that IαI impairs TSG-6–dependent ECM HA cross-linking (Fig. 3*C*, red arrowhead). HS treatment also enhanced signals of HC3 (*Itih3*) subunit (Fig. 3*C*, black arrowhead) and pre-IαI complex (Fig. 3*C*, purple arrow) signals, suggesting direct uptake by a mechanism not dependent on HA binding as the signal did not change after H'ase digestion. Therefore, to test that the IαI-HC was the substrate in serum targeted by TSG-6, we purified the IαI complex from the human serum (Enghild et al., 1989). As expected, the treatment of forebrain slices with purified IαI (400 ng/ml; 15 min) led to IαI-HC recovery after H'ase treatment (Fig. 3*D*). Purified IαI treatment stimulated uptake of pre-IαI complexes (Fig. 3*D*, purple arrow) but not HC3 subunit (Fig. 3*D*, black arrowhead). Importantly, no change in recovery after H'ase digestion was noted indicating that they do not interact with HA.

Neonatal TSG-6 expression in murine brain coincides with a time window when the blood–brain barrier is actively developing (Robertson et al., 1985; Carvey et al., 2009; Harb et al., 2013; Blanchette and Daneman, 2015; Yang et al., 2020). Hence, we next hypothesized that serum-derived IαI is present in the neonatal brain and this attenuates TSG-6–dependent ECM HA modification. To examine the impairment of TSG-6–dependent ECM HA modification, brain cortical protein lysates prepared from the postnatal developing brains were briefly treated with H'ase (1 U/ml) or left untreated. IαI-HC subunit was recovered from the postnatal brain lysates subjected to H'ase digestion consistent with the blockade of TSG-6-HA cross-linking (Fig. 3*E*, red arrowhead). The IαI antibody also detected the expression of the HC3 subunit (*Itih3*), which is constitutively expressed in the mouse brain (Zhang et al., 2016). But importantly, its levels did not change following H'ase digestion indicating that it is not associated with the ECM HA (Fig. 3*E*, black arrowhead). We further examined whether IαI-mediated ECM HA modification persists in the developing brain and found that the IαI-HC modification was not detected after P14 (Fig. 3*E*), which coincides with the maturation of the brain cerebrovascular network (Robertson et al., 1985; Harb et al., 2013; Blanchette and Daneman, 2015). To confirm that IαI-mediated HA modification is dependent on TSG-6, we prepared lysates from neonatal TSG-6$^{+/-}$ and TSG-6$^{-/-}$ brains and subjected them to H'ase digestion. IαI-HC modification was readily detectable in TSG-6$^{+/-}$ neonatal brain lysates but not in lysates from TSG-6$^{-/-}$ mice (Fig. 3*F*). Taken together, these results support that TSG-6 is active in the brain from birth onward, and the presence of serum CSPG, IαI, during a discrete window in neonatal development impairs its ECM HA cross-linking function.

TSG-6–mediated ECM modification regulates Hippo-YAP1 pathway

TSG-6–mediated modifications influence ECM HA rigidity (Baranova et al., 2011). Oligodendrocytes which express TSG-6 regulate brain ECM rigidity as well as being physiologically sensitive to changes in tissue stiffness (Segel et al., 2019; Kohnke et al., 2021; Elbaz et al., 2024). The most well known downstream sensor of changes in tissue stiffness is the RNA transcription coactivator, YAP1 (Ma et al., 2019). Mechanistically, phosphorylation of YAP1 at S127 by the Hippo kinases (Mst1/2 and Lats1/2) leads to phosphorylation and inactivation, whereas dephosphorylation activates it (Ma et al., 2019). Based on previous and our current findings, we hypothesized that TSG-6–dependent ECM HA remodeling by either cross-linking or via Iα-HC modifications differentially modulates YAP1 activity.

To determine whether Lats1 is activated in the absence of IαI-mediated HA modification in the neonatal brain, we prepared protein lysates from cortices derived from litter-matched TSG-6$^{+/+}$ and TSG-6$^{-/-}$ pups. As shown in Figure 4*A*, higher basal levels of phosphorylated Lats1 were found in lysates prepared from TSG-6$^{-/-}$ brains in contrast to TSG-6$^{+/+}$. In the same lysates, YAP1 S127 phosphorylation was enhanced in TSG-6$^{-/-}$ brains compared with TSG-6$^{+/+}$ (Fig. 4*A*). YAP1

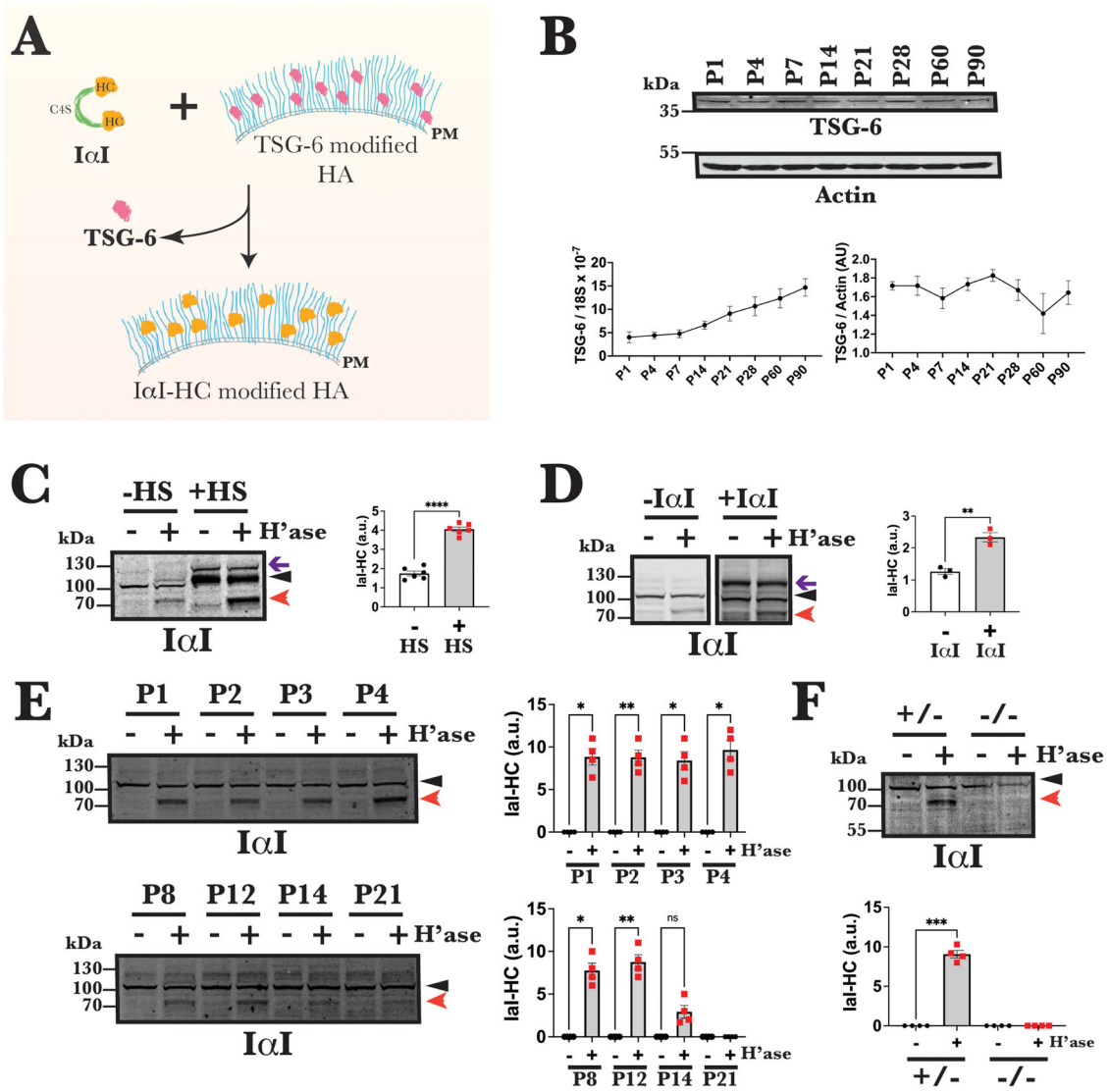

Figure 3. TSG-6–dependent ECM HA modification is impaired during a discrete neonatal window. ***A***, HC subunits of the IaI proteoglycan complex are tethered via the C4S backbone. HA (blue strands), which is tethered to the plasma membrane (PM), is cross-linked by TSG-6 resulting in ECM modification. The presence of IaI initiates a transesterification reaction leading to the release of TSG-6 from ECM HA and the transfer of IaI-HC subunits thereby modifying it. ***B***, TSG-6 protein is constitutively expressed in the mouse brain from birth to adulthood (P90; top panel). Quantification of TSG-6 protein and RNA at different ages (bottom panels). ***C***, IaI found in HS promotes ECM HA modification as significantly more IaI-HC subunit can be recovered after H'ase digestion (HS, 5%; 15 min). The forebrain slice culture protein lysates were digested with *Streptomyces* hyaluronidase (H'ase; 1 U/ml; 2 min) to release the IaI-HC subunit bound to HA (compare the − Vs + H'ase lanes). Note that the IaI antibody also detects the endogenous brain HC3 protein. The treatment with horse serum also leads to HC3 and pre-IaI uptake. IaI-HC subunit recovery quantification. ***D***, Treating forebrain slices with purified IaI (400 ng/ml; 15 min) also enhances ECM HA modification, recovery of IaI-HC subunit, and nonselective pre-IaI uptake. IaI-HC subunit recovery quantification. ***E***, The developing brain protein lysates digested with H'ase (1 U/ml; 2 min) release the IaI-HC subunit bound to HA indicating that it is remodeled from P1 to P12/14 (compare the − Vs + H'ase lanes). IaI-HC subunit recovery quantification at different ages. ***F***, ECM HA remodeling is observed in lysates prepared from P2 TSG-$6^{+/-}$ (+/—) but not litter-matched TSG-$6^{-/-}$ (−/—) brains. IaI-HC subunit recovery quantification. IaI-HC (red arrowhead); HC3 (black arrowhead); pre-IaI (purple arrow); $n = 3$ animals including both male and female (***C,D***); $n = 4$ animals (2–3 male and 1–2 female/age/genotype (***E,F***); error bars indicate ±SEM; *$p < 0.05$, **$p < 0.01$, and ****$p < 0.0001$ by paired Student's *t* test (***C–F***).

phosphorylation at Y357 (Tamm et al., 2011; Li et al., 2016) did not change between TSG-$6^{+/+}$ and TSG-$6^{-/-}$ (Fig. 4*A*) suggesting that in vivo absence of ECM HA modification does not influence Src family kinase (SFK) activation. TAZ, a YAP1 paralogue, whose levels can increase in response to loss of YAP1 function (Finch-Edmondson et al., 2015), was found to be strongly upregulated in TSG-$6^{-/-}$ brain lysates compared with TSG-$6^{+/+}$ (Fig. 4*A*). To further confirm that YAP1 phosphorylation is directly regulated by IαI-HC modification of HA, we examined its status in P16 TSG-$6^{-/-}$ brains when it can no longer be detected. Interestingly, in the samples prepared from P16 animals, we found attenuated YAP1 S127 phosphorylation in TSG-$6^{-/-}$ brain lysates compared with TSG-$6^{+/+}$ (Fig. 4*B*).

To examine whether TSG-6–mediated ECM modification-driven changes in YAP1 phosphorylation can functionally regulate its activation status, we performed luciferase assays by employing a well-characterized YAP-TEAD transcription activity reporter (Dupont et al., 2011; Azzolin et al., 2012; Yu et al., 2012). HEK293 cells were transfected with the luciferase reporter and were serum starved for 4 h and then treated with either serum alone, recombinant human TSG-6 (rhTSG-6) plus serum, rhTSG-6 alone, or Wnt3a (50 ng/ml) alone. The treatment with

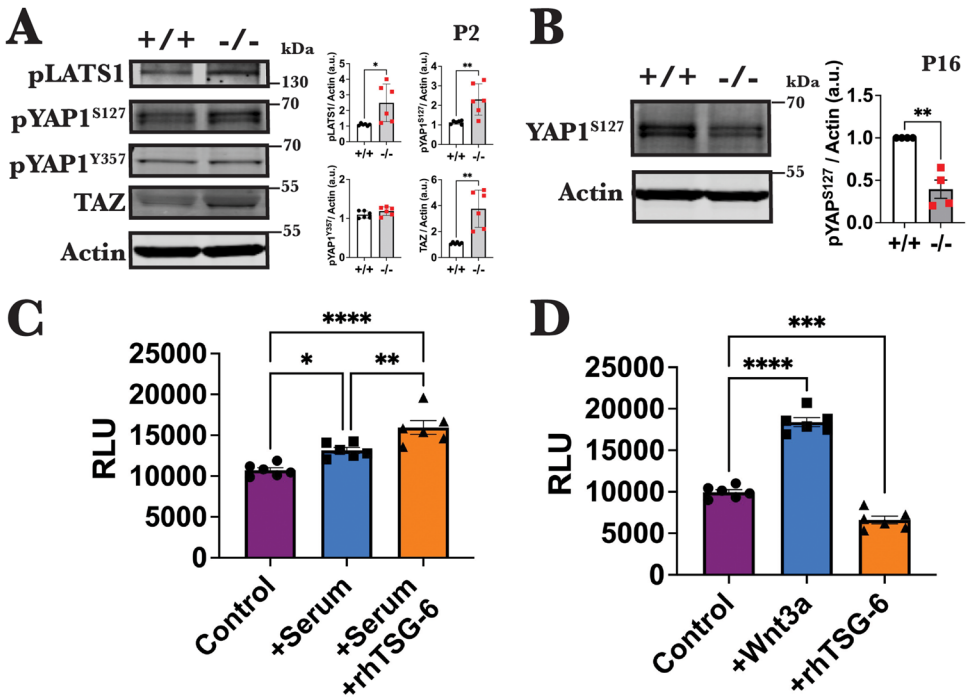

Figure 4. TSG-6–mediated ECM modification regulates Hippo-YAP1 pathway. ***A***, In the absence of HA remodeling in P2 TSG-6$^{-/-}$ brains (−/−), LATS1 and YAP1 S127 remains phosphorylated compared with litter-matched TSG-6$^{+/+}$ brains (+/+). No change in Y357 YAP1 is observed, whereas a significant increase in TAZ levels is noted. Quantification of differences in phosphorylation levels between genotypes. ***B***, At P16, TSG-6 expression ensures YAP1 S127 phosphorylation in +/+ brains. Quantification of differences in phosphorylation levels between genotypes. ***C***, HEK293 cells transfected with 8xGTIIC-luciferase plasmid (Hippo-YAP-TEAD activity reporter) stimulated with serum (5%) supplemented with rhTSG-6 (200 ng/ml) show significantly higher bioluminescent activity than serum alone. Conversely, treating the transfected cells with just rhTSG-6 leads to significant attenuation of luciferase signal compared with untreated control. Wnt3a (50 ng/ml) activation of the luciferase reporter is employed as positive control. $n = 4$–6 animals/age/genotype including both male and female (***A,B***); $n = 3$ independent experiments (***C***); error bars indicate ±SEM; $*p < 0.05$ and $**p < 0.01$ by paired Student's t test (***A,B***); $*p < 0.05$, $**p < 0.05$, $***p < 0.001$, and $****p < 0.0001$ by ANOVA (***C,D***).

serum led to a small but significant increase in signal from the reporter as previously reported (Anneren et al., 2004; Yu et al., 2012). Cotreatment with serum and rhTSG-6 led to additive response from the reporter indicating that the presence of IαI further enhanced YAP1 activation (Fig. 4*C*). The rhTSG-6 treatment without serum led to a significant decrease in luciferase signal suggesting that TSG-6 attenuates YAP1 activation in the absence of IαI (Fig. 4*D*). This attenuation was not due to nonspecific effects on cell viability as Wnt3a treatment led to a significant increase in signal from luciferase reporter in agreement with a previous report (Azzolin et al., 2012). Together, these findings suggest that TSG-6–remodeled ECM HA may serve as a homeostatic regulator of YAP1 phosphorylation status in the mouse brain: during the neonatal stage, the IαI-HC modification maintains YAP1 dephosphorylation (active), whereas from adolescence onward, TSG-6–dependent HA cross-linking stimulates phosphorylation (inactive).

YAP1 negative feedback pathways are dysregulated in TSG-6$^{-/-}$ brain

Our observations thus far support that YAP1 phosphorylation/activation can be regulated by TSG-6–mediated ECM HA modifications. However, whether this leads to changes in expression of its downstream targets is unclear. Previous findings using transgenic YAP S127A knock-in mice, in which YAP1 is constitutively active, have reported very minimal changes in expression levels of its downstream targets (Chen et al., 2015). The minimal changes in YAP1 targets in transgenic YAP S127A knock-in mice have been attributed to upregulated expression of NF2, Mst1, and Lats1 proteins, the known negative regulators of YAP1 that counteract its activation status to maintain cellular homeostasis (Chen et al., 2015; Moroishi et al., 2015). YAP1 has been identified as a regulator of amino acid metabolism via transcription of high-affinity amino acid transporters (Ibar and Irvine, 2020; Xu et al., 2023). Of particular interest is its regulation of excitatory amino acid transporter 1 (EAAT1; GLAST) and 2 (EAAT2; GLT-1) expression in the brain. Interestingly, both GLAST and GLT-1 expressions are developmentally regulated in the mouse brain (Furuta et al., 1997), but the underlying mechanisms remain unclear. GLAST protein in the cerebral cortex can be detected up to 2 weeks post birth, whereas GLT-1 protein levels gradually increase during postnatal brain development, with the earliest expression noted at P14 (Furuta et al., 1997) which coincides with the cessation of IαI-HC HA modification (Fig. 3*E*). Based on these findings, we hypothesized that the modulation of YAP1 activity by TSG-6–mediated ECM modifications is the developmental mechanism regulating GLAST and GLT-1 levels in the maturing mouse brain.

In contrast to the observations in YAP S127A knock-in mice (Chen et al., 2015), we detected significant changes in GLAST and GLT-1 expression in TSG-6$^{-/-}$ brains. We found a decrease in cortical GLAST expression from TSG-6$^{-/-}$ brain lysates at P8 (Fig. 5*A*, red arrowhead, monomer; black arrowhead, dimer). However, we noted an increase in cortical GLT-1 expression from TSG-6$^{-/-}$ brain lysates at P16 (Fig. 5*B*, red arrowhead, monomer; black arrowhead, dimer). To confirm that the changes were specific to GLT-1, we determined the expression of Connexin 30 (Cx30), which is also developmentally regulated (Kunzelmann et al., 1999). We found no changes in Cx30 expression in TSG-6$^{-/-}$ P16 or P60 brain lysates (Fig. 5*C*,*D*). Since

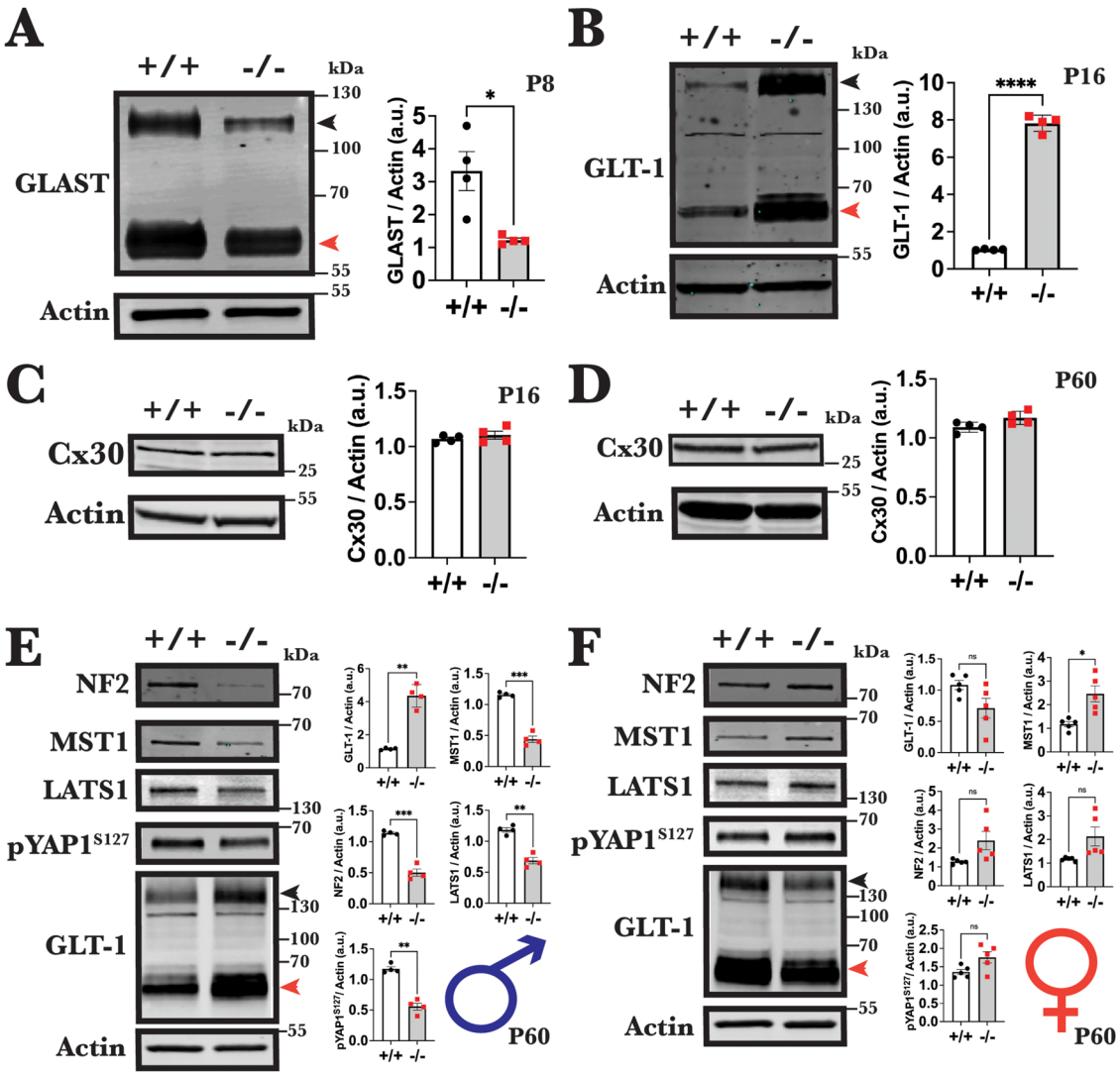

Figure 5. YAP1 negative feedback pathways are dysregulated in TSG-6$^{-/-}$ brain. ***A***, GLAST protein expression is significantly attenuated in TSG-6$^{-/-}$ (−/−) brain cortices at P8 compared with littermate TSG-6$^{+/+}$ (+/+). Quantification of differences in protein levels between the genotypes. ***B***, GLT-1 protein expression is significantly enhanced in TSG-6$^{-/-}$ (−/−) brain cortices at P16 compared with littermate TSG-6$^{+/+}$ (+/+). Quantification of differences in protein levels between the genotypes. No change in Cx30 levels is noted between +/+ and −/− at P16 (***C***) or P60 (***D***). ***E***, GLT-1 protein levels are elevated, whereas MST1, NF2, LATS1, and pYAP^{S127} levels are downregulated in TSG-6$^{-/-}$ (−/−) male cortices at P60. Differences in protein levels between the genotypes are quantified. ***F***, GLT-1 protein levels are downregulated, whereas MST1, NF2, LATS1, and pYAP^{S127} levels are elevated in TSG-6$^{-/-}$ (−/−) female cortices compared with TSG-6$^{+/+}$ (+/+) at P60. Differences in protein levels between the genotypes are quantified. GLAST and GLT-1 monomer (red arrowhead); GLAST and GLT-1 dimer (black arrowhead); $n = 4$ (3 male and 1 female)/genotype (***A,B***); $n = 4$ animals (3 males and 1 female)/genotype (***C,D***); $n = 4$ males/genotype (***E***); $n = 4$ females/genotype (***F***); error bars indicate ±SEM; $^{*}p < 0.05$, $^{**}p < 0.01$, $^{***}p < 0.001$, and $^{****}p < 0.0001$ by paired Student's *t* test (***A–F***).

GLT-1 protein level plateau during adulthood (Furuta et al., 1997), we examined adult TSG-6$^{-/-}$ mice (P60) for changes in expression. We found that GLT-1 expression remained elevated in lysates prepared from adult TSG-6$^{-/-}$ males (Fig. 5*E*), whereas GLT-1 expression in adult TSG-6$^{-/-}$ females did not differ significantly from WT females (Fig. 5*F*). Consistent with the changes seen in GLT-1, we examined and found that YAP1 S127 phosphorylation was attenuated in TSG-6$^{-/-}$ males but not females (Fig. 5*E,F*). We next checked whether the dysregulated GLT-1 expression observed in the TSG-6$^{-/-}$ male brains corresponds to perturbation of the cellular homeostatic feedback pathway, which is activated in YAP S127A knock-in mice (Chen et al., 2015; Moroishi et al., 2015). We examined the status of NF2, Lats1 and Mst1, the known negative regulators of YAP1 activity and found lower expression levels in TSG-6$^{-/-}$ male brains (Fig. 5*E*). In contrast, in TSG-6$^{-/-}$ females, except for Mst1, no significant changes in NF2 or Lats1 were noted (Fig. 5*F*). These findings suggest that TSG-6–mediated ECM HA modification is a key mechanism in the brain that regulates the developmental expression of GLAST and GLT-1. Furthermore, the failure to elicit the homeostatic control to regulate the Hippo-YAP1 pathway in TSG-6$^{-/-}$ animals implies that the dysregulation of signaling feedback may be activating other sex-dependent mechanisms to regulate YAP1 activity in the developing and mature brains.

IαI-HC ECM HA modification promotes induction of epithelial–mesenchymal transition (EMT) and inflammation

Our results support that IαI-HC ECM modification promotes YAP1 S127 dephosphorylation, whereas TSG-6–mediated cross-linking maintains phosphorylation. YAP1 S127 dephosphorylation in TSG-6$^{+/+}$ neonates and TSG-6$^{-/-}$ adults sensitizes the brain to a proinflammatory state in response to H–I injury.

Not clear from these observations is whether the proinflammatory state induced by IαI-HC ECM modifications occurs via the activation of YAP1 signaling. To test this, we employed serum-treated forebrain slice cultures prepared from TSG-$6^{+/+}$ and TSG-$6^{-/-}$ neonates and analyzed them via unbiased bulk RNA-seq for the expression of genes linked with YAP1 activation. We first determined whether serum treatment, which enhances IαI-HC ECM HA modification, leads to YAP1 activation in forebrain slice cultures. Serum exposure led to rapid dephosphorylation and inactivation of Hippo kinase LATS1 (Fig. 6*A*). However, in contrast to partial YAP1 S127 phosphorylation observed in the normal developing brain (Fig. 4*A*), serum treatment resulted in total dephosphorylation (Fig. 6*A*). Consistent with this response, we found that YAP1 phosphorylation at the SFK target site, Y357, was enhanced (Fig. 6*A*) indicating that higher concentration of serum can stimulate alternative pathways (Li et al., 2016) leading to full activation.

Given the fast-signaling kinetics leading to YAP1 dephosphorylation and activation in response to serum treatment, we restricted our bulk RNA-seq analysis to an acute 4 h treatment. To explore whether the gene expression profiles of male TSG-$6^{+/+}$ and TSG-$6^{-/-}$ display enrichment of gene sets associated with specific biological pathways, we employed the GSEA (Subramanian et al., 2005). We queried the "Hallmark" gene set category of the MSigdb. We found that the top two Hallmark pathways activated in TSG-$6^{+/+}$ forebrain slice cultures but not in those TSG-$6^{-/-}$ mice were the EMT and TNFα-NFκB pathways (Fig. 6*B*; Table 6-1). Both YAP1 and TSG-6 have been implicated as regulators of EMT (Bommaya et al., 2011; Akrida et al., 2022). The activation of EMT pathways and TNFα-NFκB signaling in the setting of mammalian brain injury exacerbates inflammation and induces a proinflammatory "myofibroblast"-like state (Singh and Singh, 2020; O'Shea et al., 2022). We next analyzed our bulk RNA-seq dataset for DEGs using the R package, DESeq2 (Love et al., 2014). Using this approach, we were able to identify 146 DEGs (Benjamin–Hochberg-adjusted $p < 0.05$) between the two serum-treated samples (Table 6-2). Genes linked with YAP1 activation and EMT promotion were significantly upregulated in TSG-$6^{+/+}$ but not TSG-$6^{-/-}$ slices: *Slc1a3* and *Ccn1* (YAP1 targets; Bertero et al., 2019; Chaqour,

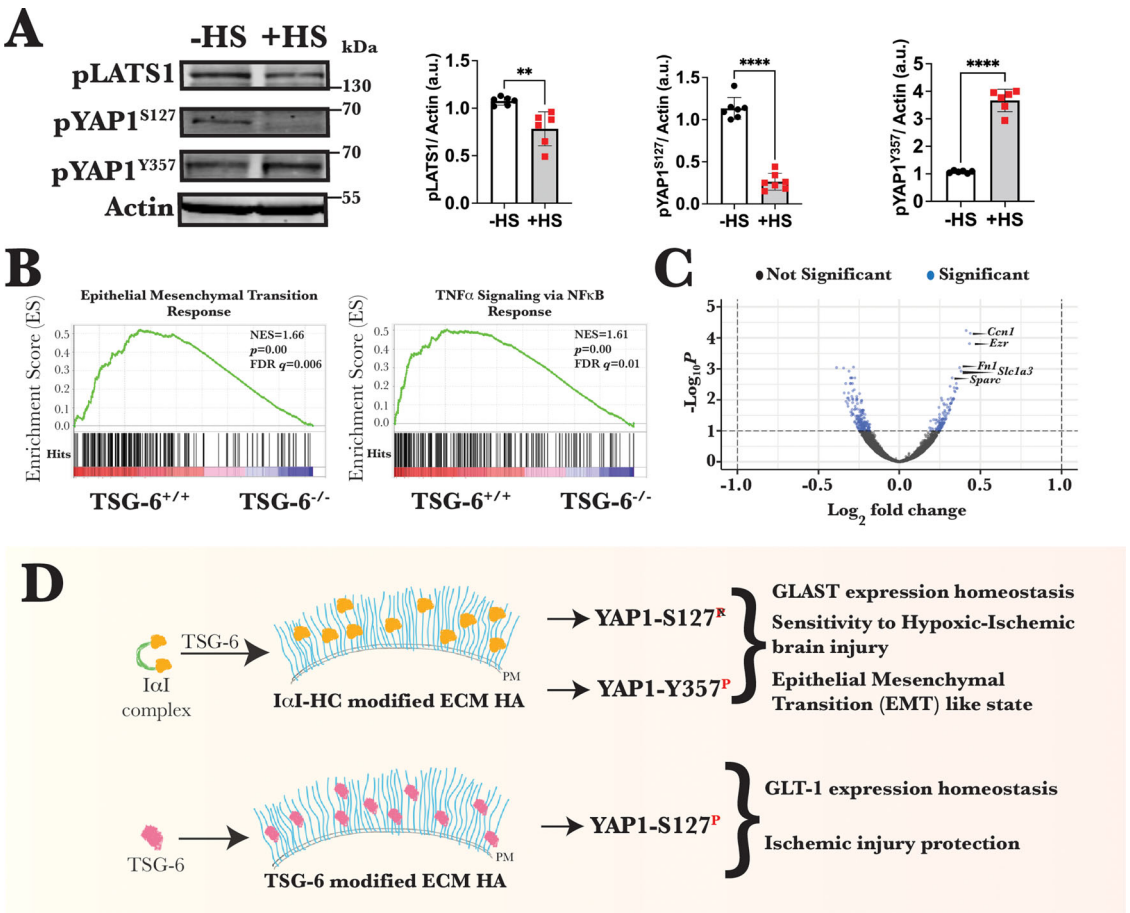

Figure 6. IαI-HC ECM HA modification promotes induction of EMT and inflammation. ***A***, Treatment with HS (15 min) leads to rapid dephosphorylation of LATS1 and YAP1 S127. In contrast to the developing brain, HS treatment enhanced YAP1 Y357 phosphorylation. Quantification of serum-mediated changes in phosphorylation. ***B***, Representative GSEA plots showing overrepresentation of Hallmark EMT_Response and TNFα_NFκB_Signaling gene sets among the DEGs for neonatal male TSG-$6^{+/+}$ and TSG-$6^{-/-}$ slice cultures treated with serum for 4 h (see Table 6-1 for details). NES and Kolmogorov–Smirnov test *p* and *q* (FDR-corrected *p*) values are indicated in graphs. ***C***, Volcano plot depicting the DEGs identified in serum-treated neonatal male TSG-$6^{-/-}$ slice cultures by DESeq2. Benjamin–Hochberg FDR-corrected $p < 0.05$ (see Table 6-2 for the complete list of DEGs and statistical details). ***D***, TSG-6–dependent ECM HA modifications serve as a novel mechanism to regulate YAP-1 activity in the brain and susceptibility to ischemic injury. (Top panel) In the presence of CSPG, IαI, TSG-6–dependent remodeling is blocked, and instead the ECM HA is modified by binding the IαI-HC subunits. This results in YAP1 S127 dephosphorylation to promote the homeostatic expression of GLAST in the developing brain. Under selective conditions that result in the activation of SFK, IαI-HC modification promotes YAP1 Y357 phosphorylation, which can sensitize the brain to H–I injury and induce an EMT-like state. (Bottom panel) In contrast, in the absence of IαI-HC modification, TSG-6 cross-links ECM HA. This modification keeps YAP1 activity in check by maintaining S127 phosphorylation to ensure homoeostatic expression of GLT-1 and may also promote neuroprotection from H–I injury. $n = 3$ from three independent experiments (***A–C***); error bars indicate ±SEM; $^{**}p < 0.01$ and $^{****}p < 0.0001$ by paired Student's *t* test (***A***).

2023) and *Ezr*, *Notch1*, *Vcam1*, *Sparc*, and *Fn1* (EMT regulators; Fig. 6*C*; Table 6-2; Zavadil et al., 2004; Kong et al., 2016; Sangaletti et al., 2016; Rout-Pitt et al., 2018; Zhang et al., 2020). Taken together, these findings support that IαI-HC ECM modification, which blocks TSG-6–dependent HA cross-linking, promotes YAP1 activation and sensitivity to ischemic injury.

Discussion

In this study, we define a novel role for TSG-6–dependent ECM modifications in homeostatic regulation of the RNA transcription coactivator, YAP1, and sensitization to H–I injury. TSG-6 expression in the brain promotes YAP1 S127 phosphorylation, and this attenuates YAP1 activity. However, in the developing brain, the presence of CSPG, IαI, instead blocks TSG-6–dependent ECM modification, which enhances YAP1 S127 dephosphorylation leading to YAP1 activation. Our findings suggest that these TSG-6–mediated ECM HA modifications have functional consequences, which ensure timely expression of excitatory amino acid transporter(s) during maturation and regulate the inflammatory response to H–I injury.

In all tissues examined to date, TSG-6 expression is upregulated in response to inflammation and injury but is undetectable under normal homeostatic conditions (Day and Milner, 2019). We find that in the mouse brain, TSG-6 is active from birth onward, and during a discrete neurodevelopmental window, the serum CSPG, IαI, blocks TSG-6–dependent ECM HA modification. This blockade of TSG-6–dependent ECM HA remodeling by IαI coincides with a period when low levels of serum proteins have been shown to leak across the maturing BBB (Robertson et al., 1985; Harb et al., 2013; Blanchette and Daneman, 2015; Yang et al., 2020). Low levels of serum proteins are required for the differentiation of NPCs in the postnatal mouse brain, whereas higher concentrations induce the expression of genes activating EMT and proinflammatory pathways (O'Shea et al., 2022). Our in vitro (forebrain slice cultures and RNA-seq) and in vivo (H–I injury) studies analyzed the conditions where the serum enhances IαI-HC–dependent blockade of TSG-6–mediated ECM HA remodeling. These complementary approaches support a sex-dependent neuroprotective role for TSG-6 in the adult brain. Interestingly, the administration of superphysiological concentrations of recombinant IαI promotes neuroprotection and behavioral recovery in various rodent H–I models by repairing BBB damage and attenuating influx of peripheral immune cells into the brain parenchyma (Koehn et al., 2020; McCullough et al., 2021). It is possible that neuroprotection by recombinant IαI may also be mediated through an interaction with the soluble pattern recognition receptor, Pentraxin 3 (PTX3), which alters TSG-6-dependent ECM HA modification (Baranova et al., 2014) thereby influencing downstream activation of YAP1. Future studies will determine whether systemic administration of IαI in rodents can exert its neuroprotective activity without interfering with TSG-6–dependent ECM HA modification.

Mechanistically, TSG-6 functions to cross-link HA and rigidify the ECM, but the presence of IαI blocks these modifications and promotes softening of the ECM (Baranova et al., 2011, 2013). YAP1 activity is sensitive to changes in extracellular rigidity (Dupont et al., 2011); therefore, our results establish TSG-6–dependent ECM HA modifications as a unique homeostatic signaling effector (Fig. 6*E*). This homeostatic regulation of YAP1 activation by TSG-6–mediated ECM remodeling in the presence and absence of IαI confers in the brain the functionality to modulate the timely developmental expression of excitatory amino acid transporters, GLAST and GLT-1 (Ibar and Irvine, 2020). Prior studies have identified YAP1 as a member of transcription factor modules that regulate inflammation during spinal cord injury (Burda et al., 2022). Our results support that the neonatal blockade of TSG-6–dependent ECM HA remodeling by IαI promotes total YAP1 activation via signaling by both Hippo and SFK pathways, which induces an EMT-like state, hypertrophic morphological transformation, and inflammation. Furthermore, the enrichment of E2F target gene sets after a 24 h treatment with serum suggests a role for YAP1 as it has been shown to cooperate with E2F transcription factors (Nicolay et al., 2011; Kapoor et al., 2014). Both TSG-6 and YAP1 have been linked to induction of EMT states (Bommaya et al., 2011; Akrida et al., 2022). Interestingly, the activation of YAP1 in a zebrafish spinal cord injury model also induces an EMT-like state, which promotes the formation of "bridging" cells that mediate lesion repair (Klatt Shaw et al., 2021). We find that in the setting of attenuated YAP1 activation in neonatal TSG-$6^{-/-}$ brains, H–I injury promoted the generation of palisading $GFAP^{+}$ astrocytes, which are proposed to have anti-inflammatory and repair promoting properties (Faulkner et al., 2004). However, in the setting of YAP1 activation in adult TSG-$6^{-/-}$ brains, H–I injury promoted the generation of more hypertrophic $GFAP^{+}$ astrocytes. This suggests a common conserved YAP1-dependent response to injury or inflammation but is regulated in multiple ways, possibly due to different selection pressures during chordate evolution. Furthermore, these findings suggest the existence of transcription factor modules that integrate YAP1 activation by multiple different pathways to regulate anti- and proinflammatory pathways in an age- and sex-dependent manner. Since YAP1 S127 phosphorylation is regulated by ECM HA modifications, it may be feasible to develop either IαI or TSG-6–based therapies to differentially modulate YAP1 activity in response to ischemic brain injury to regulate anti- and proinflammatory pathways in an age- and sex-dependent manner.

YAP1 activity is tightly regulated in vivo. Observations from transgenic YAP1 S127A mice, where it is constitutively activated, indicate minimal changes in the expression of downstream targets due to the upregulation of negative modulators (Chen et al., 2015; Moroishi et al., 2015). Negative feedback regulation of upstream pathway components is a common feature of many signaling pathways that is generally believed to contribute to the steadiness and robustness of cell signaling in vivo (Stelling et al., 2004). In contrast to the findings from transgenic YAP S127A animals, we found that dysregulated YAP1 activation in TSG-$6^{-/-}$ males led to significant changes in the expression of the downstream YAP1 targets GLAST and GLT-1. Furthermore, we did not detect the upregulation of negative Hippo pathway regulators like Mst1, Lats1, and NF2. Therefore, our results are conceptually similar to that previously described in *Drosophila*, where increasing or decreasing Yorkie (Yki; YAP1) activity is accompanied by changes in the expression of downstream targets without negative feedback regulation (Cho et al., 2006; Hamaratoglu et al., 2006; Genevet et al., 2010).

GLT-1 is the most abundantly expressed protein in the brain and plays a critical role in regulating glutamate transport during normal homeostatic conditions and in injury settings to provide protection from excitotoxicity (Rimmele et al., 2021). We found dysregulated GLT-1 expression in TSG-$6^{-/-}$ animals was sustained from adolescence to adulthood. Although GLT-1 can mediate a neuroprotective role when its expression

is enhanced prior to H–I injury (Chu et al., 2007), our results on the other hand suggest that high GLT-1 expression in adult TSG-$6^{-/-}$ males was unable to confer neuroprotection. This suggests that dysregulated GLT-1 expression in TSG-$6^{-/-}$ brains may contribute to enhanced excitotoxicity via mechanisms possibly involving reverse transport (Tekkok et al., 2007). Sex is a key risk factor that influences stroke susceptibility (Roy-O'Reilly and McCullough, 2018); future studies will determine whether dysregulated GLT-1 expression and/or function contributes to aberrant regulation of glutamate homeostasis as an explanation for the increased susceptibility of TSG-$6^{-/-}$ males to ischemic injury.

Our study was limited by a lack of availability of selective antibodies to identify the IαI-HC subunit that interacts with HA. In addition, we partially addressed the role of YAP1 activation in the regulation of GLT-1 expression and did not examine its contribution as a member of different transcription factor modules. Our transcriptomic analysis of forebrain slices only examined the impact of HA modification on the activation of early responding inflammatory and neuroprotective pathways. While we demonstrated a role for TSG-6 expression in regulating age-dependent ischemic injury outcomes, this dependence could be influenced in part by the degree of the insult and distribution of lesions between the neonates and adults. Finally, our genetic model (TSG-$6^{-/-}$) does not target the ECM of any specific cell type, and modifying homeostatic HA signaling selectively in the oligodendrocytes, astrocytes, and/or neurons may provide further insight into their relative contributions to regulate the ischemic injury response.

In summary, we show that constitutive expression of TSG-6 in the brain broadens the role of HA beyond an inert biophysical support scaffold that provides bioactive polysaccharides during inflammation. We demonstrate that TSG-6 expression throughout life enables it to function as a homeostatic signaling effector and that its regulation of YAP1 phosphorylation in the developing and adult injured brain contributes to ischemic injury responses in a maturation-dependent fashion. Furthermore, our findings suggest that manipulating ECM HA modification via IαI or TSG-6 could provide a powerful new means to differentially regulate sex-dependent inflammatory pathways to promote repair and regeneration in response to ischemic stroke in neonates and adults.

Data Availability

The RNA-seq dataset containing the aligned raw reads for each sample from both the 4 and 24 h serum treatments and the normalized counts for all the detected genes has been deposited to the Gene Expression Omnibus, Accession Number GSE249085. The data is currently private and can accessed by the reviewers using the link and unique token as follows: https://urldefense.com/v3/__https://www.ncbi.nlm.nih.gov/geo/query/acc.cgi?acc=GSE249085__;!!Mi0JBg!NLKBivIzdSJ9ZiJU4WOPNhlaLfSab1OROzHYIXbuzBeMS6tYYEx47Dcpa3WDNYHPWTnQMM7XJ5NiGWP9Ll0$

token: spoxymcobtgjjej.

References

Akrida I, Bravou V, Papadaki H (2022) The deadly cross-talk between Hippo pathway and epithelial-mesenchymal transition (EMT) in cancer. Mol Biol Rep 49:10065–10076.

Anneren C, Cowan CA, Melton DA (2004) The Src family of tyrosine kinases is important for embryonic stem cell self-renewal. J Biol Chem 279: 31590–31598.

Asher RA, Morgenstern DA, Shearer MC, Adcock KH, Pesheva P, Fawcett JW (2002) Versican is upregulated in CNS injury and is a product of oligodendrocyte lineage cells. J Neurosci 22:2225–2236.

Azzolin L, Zanconato F, Bresolin S, Forcato M, Basso G, Bicciato S, Cordenonsi M, Piccolo S (2012) Role of TAZ as mediator of Wnt signaling. Cell 151:1443–1456.

Back SA, et al. (2005) Hyaluronan accumulates in demyelinated lesions and inhibits oligodendrocyte progenitor maturation. Nat Med 11:966–972.

Back SA (2017) White matter injury in the preterm infant: pathology and mechanisms. Acta Neuropathol 134:331–349.

Bano F, Tammi MI, Kang DW, Harris EN, Richter RP (2018) Single-molecule unbinding forces between the polysaccharide hyaluronan and its binding proteins. Biophys J 114:2910–2922.

Baranova NS, Foulcer SJ, Briggs DC, Tilakaratna V, Enghild JJ, Milner CM, Day AJ, Richter RP (2013) Inter-alpha-inhibitor impairs TSG-6-induced hyaluronan cross-linking. J Biol Chem 288:29642–29653.

Baranova NS, Inforzato A, Briggs DC, Tilakaratna V, Enghild JJ, Thakar D, Milner CM, Day AJ, Richter RP (2014) Incorporation of pentraxin 3 into hyaluronan matrices is tightly regulated and promotes matrix cross-linking. J Biol Chem 289:30481–30498.

Baranova NS, Nileback E, Haller FM, Briggs DC, Svedhem S, Day AJ, Richter RP (2011) The inflammation-associated protein TSG-6 cross-links hyaluronan via hyaluronan-induced TSG-6 oligomers. J Biol Chem 286: 25675–25686.

Bederson JB, Pitts LH, Germano SM, Nishimura MC, Davis RL, Bartkowski HM (1986) Evaluation of 2,3,5-triphenyltetrazolium chloride as a stain for detection and quantification of experimental cerebral infarction in rats. Stroke 17:1304–1308.

Bertero T, et al. (2019) Tumor-stroma mechanics coordinate amino acid availability to sustain tumor growth and malignancy. Cell Metab 29: 124–140.e10.

Bertling F, Bendix I, Drommelschmidt K, Wisniewski HG, Felderhoff-Mueser U, Keller M, Prager S (2016) Tumor necrosis factor-inducible gene 6 protein: a novel neuroprotective factor against inflammation-induced developmental brain injury. Exp Neurol 279:283–289.

Blanchette M, Daneman R (2015) Formation and maintenance of the BBB. Mech Dev 138:8–16.

Bogie JFJ, Haidar M, Kooij G, Hendriks JJA (2020) Fatty acid metabolism in the progression and resolution of CNS disorders. Adv Drug Deliv Rev 159: 198–213.

Bommaya G, Meran S, Krupa A, Phillips AO, Steadman R (2011) Tumour necrosis factor-stimulated gene (TSG)-6 controls epithelial-mesenchymal transition of proximal tubular epithelial cells. Int J Biochem Cell Biol 43: 1739–1746.

Burda JE, et al. (2022) Divergent transcriptional regulation of astrocyte reactivity across disorders. Nature 606:557–564.

Carvey PM, Hendey B, Monahan AJ (2009) The blood-brain barrier in neurodegenerative disease: a rhetorical perspective. J Neurochem 111:291–314.

Chaqour B (2023) CCN-Hippo YAP signaling in vision and its role in neuronal, glial and vascular cell function and behavior. J Cell Commun Signal 17:255–262.

Chen Q, et al. (2015) Homeostatic control of Hippo signaling activity revealed by an endogenous activating mutation in YAP. Genes Dev 29:1285–1297.

Cho E, Feng Y, Rauskolb C, Maitra S, Fehon R, Irvine KD (2006) Delineation of a fat tumor suppressor pathway. Nat Genet 38:1142–1150.

Chu K, et al. (2007) Pharmacological induction of ischemic tolerance by glutamate transporter-1 (EAAT2) upregulation. Stroke 38:177–182.

Coulson-Thomas VJ, Lauer ME, Soleman S, Zhao C, Hascall VC, Day AJ, Fawcett JW (2016) Tumor necrosis factor-stimulated gene-6 (TSG-6) is constitutively expressed in adult central nervous system (CNS) and associated with astrocyte-mediated glial scar formation following spinal cord injury. J Biol Chem 291:19939–19952.

Cui S, Ke L, Wang H, Li L (2023) TSG-6 alleviates cerebral ischemia/reperfusion injury and blood-brain barrier disruption by suppressing ER stress-mediated inflammation. Brain Res 1817:148466.

Davoust N, Jones J, Stahel PF, Ames RS, Barnum SR (1999) Receptor for the C3a anaphylatoxin is expressed by neurons and glial cells. Glia 26:201–211.

Day AJ, Milner CM (2019) TSG-6: a multifunctional protein with anti-inflammatory and tissue-protective properties. Matrix Biol 78–79:60–83.

Di Santo C, La Russa D, Greco R, Persico A, Zanaboni AM, Bagetta G, Amantea D (2023) Characterization of the involvement of tumour

necrosis factor (TNF)-alpha-stimulated gene 6 (TSG-6) in ischemic brain injury caused by middle cerebral artery occlusion in mouse. Int J Mol Sci 24:5800.
Dupont S, et al. (2011) Role of YAP/TAZ in mechanotransduction. Nature 474:179–183.
Elbaz B, Darwish A, Vardy M, Isaac S, Tokars HM, Dzhashiashvili Y, Korshunov K, Prakriya M, Eden A, Popko B (2024) The bone transcription factor Osterix controls extracellular matrix- and node of Ranvier-related gene expression in oligodendrocytes. Neuron 112:247–263.e6.
Enghild JJ, Thogersen IB, Pizzo SV, Salvesen G (1989) Analysis of inter-alpha-trypsin inhibitor and a novel trypsin inhibitor, pre-alpha-trypsin inhibitor, from human plasma. Polypeptide chain stoichiometry and assembly by glycan. J Biol Chem 264:15975–15981.
Fard MK, et al. (2017) BCAS1 expression defines a population of early myelinating oligodendrocytes in multiple sclerosis lesions. Sci Transl Med 9: 7816.
Fasanello DC, et al. (2021) Hyaluronic acid synthesis, degradation, and cross-linking in equine osteoarthritis: TNF-alpha-TSG-6-mediated HC-HA formation. Arthritis Res Ther 23:218.
Faulkner JR, Herrmann JE, Woo MJ, Tansey KE, Doan NB, Sofroniew MV (2004) Reactive astrocytes protect tissue and preserve function after spinal cord injury. J Neurosci 24:2143–2155.
Feigin VL, Brainin M, Norrving B, Martins S, Sacco RL, Hacke W, Fisher M, Pandian J, Lindsay P (2022) World stroke organization (WSO): global stroke fact sheet 2022. Int J Stroke 17:18–29.
Ferriero DM (2004) Neonatal brain injury. N Engl J Med 351:1985–1995.
Finch-Edmondson ML, Strauss RP, Passman AM, Sudol M, Yeoh GC, Callus BA (2015) TAZ protein accumulation is negatively regulated by YAP abundance in mammalian cells. J Biol Chem 290:27928–27938.
Furuta A, Rothstein JD, Martin LJ (1997) Glutamate transporter protein subtypes are expressed differentially during rat CNS development. J Neurosci 17:8363–8375.
Gasque P (2004) Complement: a unique innate immune sensor for danger signals. Mol Immunol 41:1089–1098.
Genevet A, Wehr MC, Brain R, Thompson BJ, Tapon N (2010) Kibra is a regulator of the Salvador/Warts/Hippo signaling network. Dev Cell 18:300–308.
Haas S, Steplewski A, Siracusa LD, Amini S, Khalili K (1995) Identification of a sequence-specific single-stranded DNA binding protein that suppresses transcription of the mouse myelin basic protein gene. J Biol Chem 270: 12503–12510.
Hamaratoglu F, Willecke M, Kango-Singh M, Nolo R, Hyun E, Tao C, Jafar-Nejad H, Halder G (2006) The tumour-suppressor genes NF2/Merlin and expanded act through Hippo signalling to regulate cell proliferation and apoptosis. Nat Cell Biol 8:27–36.
Harb R, Whiteus C, Freitas C, Grutzendler J (2013) In vivo imaging of cerebral microvascular plasticity from birth to death. J Cereb Blood Flow Metab 33:146–156.
Hickman S, Izzy S, Sen P, Morsett L, El Khoury J (2018) Microglia in neurodegeneration. Nat Neurosci 21:1359–1369.
Ibar C, Irvine KD (2020) Integration of Hippo-YAP signaling with metabolism. Dev Cell 54:256–267.
Jarlestedt K, et al. (2013) Receptor for complement peptide C3a: a therapeutic target for neonatal hypoxic-ischemic brain injury. FASEB J 27:3797–3804.
Jiang X, Andjelkovic AV, Zhu L, Yang T, Bennett MVL, Chen J, Keep RF, Shi Y (2018) Blood-brain barrier dysfunction and recovery after ischemic stroke. Prog Neurobiol 163–164:144–171.
Kapoor A, et al. (2014) Yap1 activation enables bypass of oncogenic Kras addiction in pancreatic cancer. Cell 158:185–197.
Killoy KM, Harlan BA, Pehar M, Vargas MR (2020) FABP7 upregulation induces a neurotoxic phenotype in astrocytes. Glia 68:2693–2704.
Kipp M, Clarner T, Gingele S, Pott F, Amor S, van der Valk P, Beyer C (2011) Brain lipid binding protein (FABP7) as modulator of astrocyte function. Physiol Res 60:S49–S60.
Klatt Shaw D, Saraswathy VM, Zhou L, McAdow AR, Burris B, Butka E, Morris SA, Dietmann S, Mokalled MH (2021) Localized EMT reprograms glial progenitors to promote spinal cord repair. Dev Cell 56:613–626.e7.
Koehn LM, Chen X, Logsdon AF, Lim YP, Stonestreet BS (2020) Novel neuroprotective agents to treat neonatal hypoxic-ischemic encephalopathy: inter-alpha inhibitor proteins. Int J Mol Sci 21:9193.
Kohnke S, et al. (2021) Nutritional regulation of oligodendrocyte differentiation regulates perineuronal net remodeling in the median eminence. Cell Rep 36:109362.
Kong J, Di C, Piao J, Sun J, Han L, Chen L, Yan G, Lin Z (2016) Ezrin contributes to cervical cancer progression through induction of epithelial-mesenchymal transition. Oncotarget 7:19631–19642.
Kunzelmann P, Schroder W, Traub O, Steinhauser C, Dermietzel R, Willecke K (1999) Late onset and increasing expression of the gap junction protein connexin30 in adult murine brain and long-term cultured astrocytes. Glia 25:111–119.
Lalancette-Hebert M, Gowing G, Simard A, Weng YC, Kriz J (2007) Selective ablation of proliferating microglial cells exacerbates ischemic injury in the brain. J Neurosci 27:2596–2605.
Lattke M, Goldstone R, Ellis JK, Boeing S, Jurado-Arjona J, Marichal N, MacRae JI, Berninger B, Guillemot F (2021) Extensive transcriptional and chromatin changes underlie astrocyte maturation in vivo and in culture. Nat Commun 12:4335.
Lauer ME, Loftis J, de la Motte C, Hascall VC (2015) Analysis of the heavy-chain modification and TSG-6 activity in pathological hyaluronan matrices. Methods Mol Biol 1229:543–548.
Li P, Silvis MR, Honaker Y, Lien WH, Arron ST, Vasioukhin V (2016) AlphaE-catenin inhibits a Src-YAP1 oncogenic module that couples tyrosine kinases and the effector of Hippo signaling pathway. Genes Dev 30: 798–811.
Lian H, Litvinchuk A, Chiang AC, Aithmitti N, Jankowsky JL, Zheng H (2016) Astrocyte-microglia cross talk through complement activation modulates amyloid pathology in mouse models of Alzheimer's disease. J Neurosci 36:577–589.
Liddelow SA, Barres BA (2017) Reactive astrocytes: production, function, and therapeutic potential. Immunity 46:957–967.
Lodygensky GA, West T, Moravec MD, Back SA, Dikranian K, Holtzman DM, Neil JJ (2011) Diffusion characteristics associated with neuronal injury and glial activation following hypoxia-ischemia in the immature brain. Magn Reson Med 66:839–845.
Love MI, Huber W, Anders S (2014) Moderated estimation of fold change and dispersion for RNA-seq data with DESeq2. Genome Biol 15:550.
Ma Q (2013) Role of nrf2 in oxidative stress and toxicity. Annu Rev Pharmacol Toxicol 53:401–426.
Ma S, Meng Z, Chen R, Guan KL (2019) The Hippo pathway: biology and pathophysiology. Annu Rev Biochem 88:577–604.
MacManus JP, Jian M, Preston E, Rasquinha I, Webster J, Zurakowski B (2003) Absence of the transcription factor E2F1 attenuates brain injury and improves behavior after focal ischemia in mice. J Cereb Blood Flow Metab 23:1020–1028.
Mayes DA, et al. (2013) Nf1 loss and Ras hyperactivation in oligodendrocytes induce NOS-driven defects in myelin and vasculature. Cell Rep 4:1197–1212.
McCullough LD, et al. (2021) Exogenous inter-alpha inhibitor proteins prevent cell death and improve ischemic stroke outcomes in mice. J Clin Invest 131:e144898.
Millar LJ, Shi L, Hoerder-Suabedissen A, Molnar Z (2017) Neonatal hypoxia ischaemia: mechanisms, models, and therapeutic challenges. Front Cell Neurosci 11:78.
Milner CM, Day AJ (2003) TSG-6: a multifunctional protein associated with inflammation. J Cell Sci 116:1863–1873.
Moroishi T, et al. (2015) A YAP/TAZ-induced feedback mechanism regulates Hippo pathway homeostasis. Genes Dev 29:1271–1284.
Nicolay BN, Bayarmagnai B, Islam AB, Lopez-Bigas N, Frolov MV (2011) Cooperation between dE2F1 and Yki/Sd defines a distinct transcriptional program necessary to bypass cell cycle exit. Genes Dev 25:323–335.
O'Shea TM, Ao Y, Wang S, Wollenberg AL, Kim JH, Ramos Espinoza RA, Czechanski A, Reinholdt LG, Deming TJ, Sofroniew MV (2022) Lesion environments direct transplanted neural progenitors towards a wound repair astroglial phenotype in mice. Nat Commun 13:5702.
Rimmele TS, et al. (2021) Neuronal loss of the glutamate transporter GLT-1 promotes excitotoxic injury in the hippocampus. Front Cell Neurosci 15: 788262.
Robertson PL, Du Bois M, Bowman PD, Goldstein GW (1985) Angiogenesis in developing rat brain: an in vivo and in vitro study. Brain Res 355:219–223.
Rout-Pitt N, Farrow N, Parsons D, Donnelley M (2018) Epithelial mesenchymal transition (EMT): a universal process in lung diseases with implications for cystic fibrosis pathophysiology. Respir Res 19:136.
Roy-O'Reilly M, McCullough LD (2018) Age and sex are critical factors in ischemic stroke pathology. Endocrinology 159:3120–3131.

Salier JP, Rouet P, Raguenez G, Daveau M (1996) The inter-alpha-inhibitor family: from structure to regulation. Biochem J 315:1–9.
Sangaletti S, et al. (2016) Mesenchymal transition of high-grade breast carcinomas depends on extracellular matrix control of myeloid suppressor cell activity. Cell Rep 17:233–248.
Sanggaard KW, Hansen L, Scavenius C, Wisniewski HG, Kristensen T, Thogersen IB, Enghild JJ (2010) Evolutionary conservation of heavy chain protein transfer between glycosaminoglycans. Biochim Biophys Acta 1804:1011–1019.
Segel M, et al. (2019) Niche stiffness underlies the ageing of central nervous system progenitor cells. Nature 573:130–134.
Sharifi K, et al. (2011) FABP7 expression in normal and stab-injured brain cortex and its role in astrocyte proliferation. Histochem Cell Biol 136: 501–513.
Singh S, Singh TG (2020) Role of nuclear factor kappa B (NF-kappaB) signalling in neurodegenerative diseases: an mechanistic approach. Curr Neuropharmacol 18:918–935.
Spicer AP, Joo A, Bowling RA Jr (2003) A hyaluronan binding link protein gene family whose members are physically linked adjacent to chondroitin sulfate proteoglycan core protein genes: the missing links. J Biol Chem 278:21083–21091.
Srivastava T, et al. (2018) A TLR/AKT/FoxO3 immune tolerance-like pathway disrupts the repair capacity of oligodendrocyte progenitors. J Clin Invest 128:2025–2041.
Stelling J, Sauer U, Szallasi Z, Doyle FJ 3rd, Doyle J (2004) Robustness of cellular functions. Cell 118:675–685.
Subramanian A, et al. (2005) Gene set enrichment analysis: a knowledge-based approach for interpreting genome-wide expression profiles. Proc Natl Acad Sci U S A 102:15545–15550.
Tabula Muris Consortium, Overall Coordination, Logistical coordination, Organ collection and processing, Library preparation and sequencing, Computational data analysis, Cell type annotation, Writing group, Supplemental text writing group, Principal investigators (2018) Single-cell transcriptomics of 20 mouse organs creates a Tabula Muris. Nature 562:367–372.
Tamm C, Bower N, Anneren C (2011) Regulation of mouse embryonic stem cell self-renewal by a Yes-YAP-TEAD2 signaling pathway downstream of LIF. J Cell Sci 124:1136–1144.
Tekkok SB, Ye Z, Ransom BR (2007) Excitotoxic mechanisms of ischemic injury in myelinated white matter. J Cereb Blood Flow Metab 27:1540–1552.
Vannucci SJ, Back SA (2022) The Vannucci model of hypoxic-ischemic injury in the neonatal rodent: 40 years later. Dev Neurosci 44:186–193.
Wu F, Zou Q, Ding X, Shi D, Zhu X, Hu W, Liu L, Zhou H (2016) Complement component C3a plays a critical role in endothelial activation and leukocyte recruitment into the brain. J Neuroinflammation 13:23.
Xu X, et al. (2023) Yes-associated protein regulates glutamate homeostasis through promoting the expression of excitatory amino acid transporter-2 in astrocytes via beta-catenin signaling. Glia 71:1197–1216.
Yamada H, Fredette B, Shitara K, Hagihara K, Miura R, Ranscht B, Stallcup WB, Yamaguchi Y (1997) The brain chondroitin sulfate proteoglycan brevican associates with astrocytes ensheathing cerebellar glomeruli and inhibits neurite outgrowth from granule neurons. J Neurosci 17: 7784–7795.
Yang AC, et al. (2020) Physiological blood-brain transport is impaired with age by a shift in transcytosis. Nature 583:425–430.
Yu FX, et al. (2012) Regulation of the hippo-YAP pathway by G-protein-coupled receptor signaling. Cell 150:780–791.
Zavadil J, Cermak L, Soto-Nieves N, Bottinger EP (2004) Integration of TGF-beta/smad and Jagged1/Notch signalling in epithelial-to-mesenchymal transition. EMBO J 23:1155–1165.
Zhang Y, et al. (2016) Purification and characterization of progenitor and mature human astrocytes reveals transcriptional and functional differences with mouse. Neuron 89:37–53.
Zhang D, et al. (2020) VCAM1 promotes tumor cell invasion and metastasis by inducing EMT and transendothelial migration in colorectal cancer. Front Oncol 10:1066.
Zhu W, Libal NL, Casper A, Bodhankar S, Offner H, Alkayed NJ (2014) Recombinant T cell receptor ligand treatment improves neurological outcome in the presence of tissue plasminogen activator in experimental ischemic stroke. Transl Stroke Res 5:612–617.